AD-A058 614 RHODE ISLAND UNIV KINGSTON DEPT OF OCEAN ENGINEERING F/G 11/6
RAMAN AND INFRARED SPECTROSCOPY OF AQUEOUS CORROSION FILMS ON L--ETC(U)
AUG 78 R H HEIDERSBACH, C W BROWN N00014-76-C-0889
UNCLASSIFIED TR-4 NL

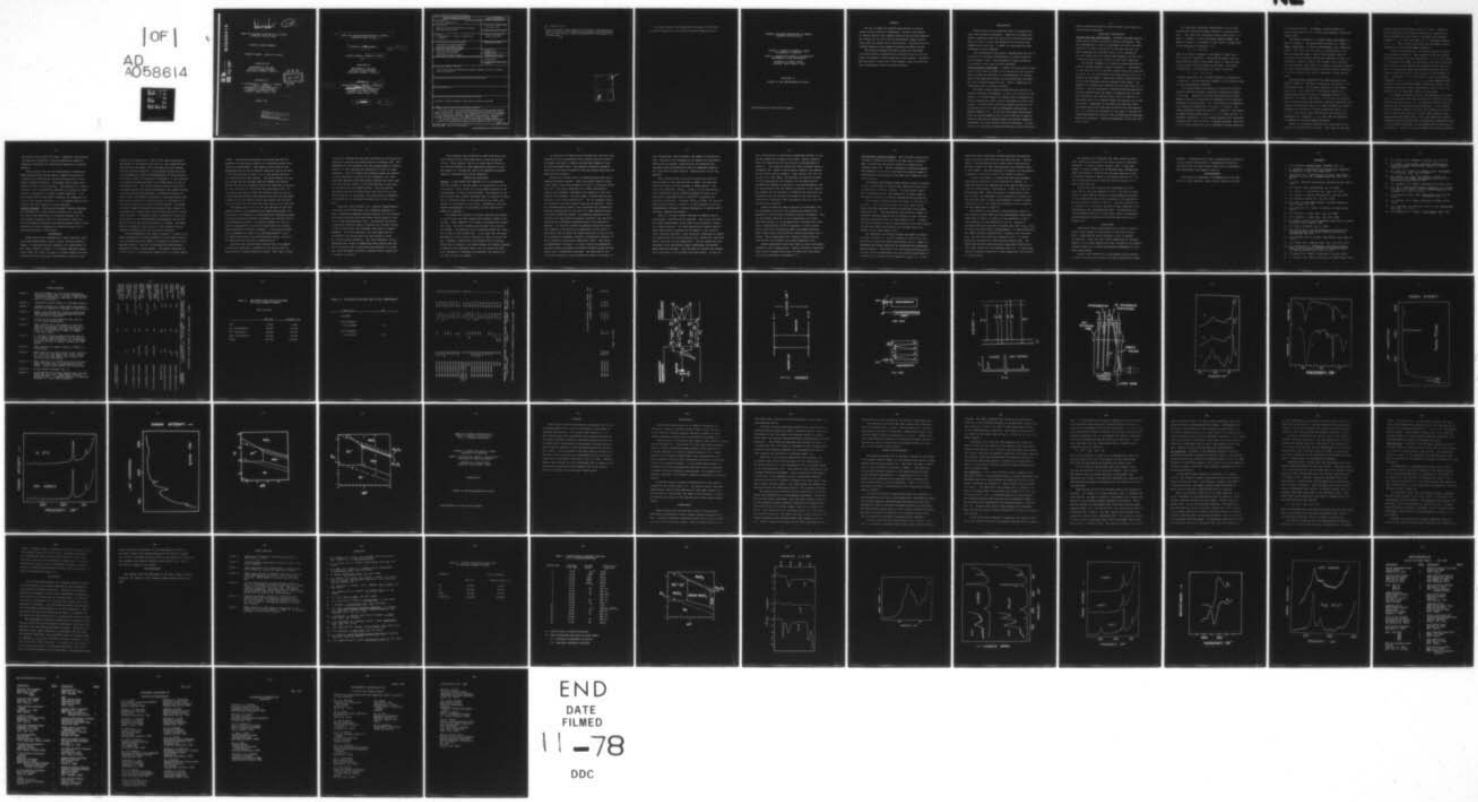

END
DATE FILMED
11-78
DDC

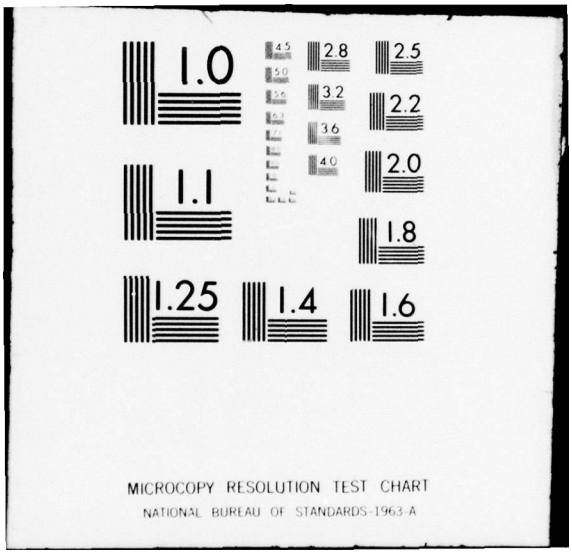
1.0
1.1
1.25
1.4
1.6
1.8
2.0
2.2
2.5
2.8
3.2
3.6
4.0
4.5
5.0
5.6
6.3
MICROCOPY RESOLUTION TEST CHART
NATIONAL BUREAU OF STANDARDS-1963-A

LEVEL II

12

RAMAN AND INFRARED SPECTROSCOPY OF AQUEOUS CORROSION FILMS ON LEAD

TECHNICAL REPORT NUMBER 4

CONTRACT NUMBER: N00014-76-c-0889

SUBMITTED TO:

DEPARTMENT OF THE NAVY
OFFICE OF NAVAL RESEARCH
METALLURGY PROGRAM - CODE 471

PREPARED BY:

R. HEIDERSBACH, C. BROWN, R. THIBEAU
AND A. GOLDFARB
DEPARTMENT OF OCEAN ENGINEERING
UNIVERSITY OF RHODE ISLAND
KINGSTON, RHODE ISLAND 02881

AUGUST 1978

(6) RAMAN AND INFRARED SPECTROSCOPY OF AQUEOUS CORROSION FILMS ON LEAD

(9) TECHNICAL REPORT NUMBER 4

(14) TR-4

CONTRACT NUMBER: (15) N00014-76-c-0889

SUBMITTED TO:

DEPARTMENT OF THE NAVY
OFFICE OF NAVAL RESEARCH
METALLURGY PROGRAM - CODE 471

PREPARED BY:

(10) Robert H. [redacted] HEIDERSBACH, C. W. BROWN, R. J. THIBEAU
Arnon Z. [redacted] GOLDFARB
DEPARTMENT OF OCEAN ENGINEERING
UNIVERSITY OF RHODE ISLAND
KINGSTON, RHODE ISLAND 02881

(11) AUG [redacted] 78

(12) 73 p.

407 892

mt

SECURITY CLASSIFICATION OF THIS PAGE (When Data Entered)

REPORT DOCUMENTATION PAGE

READ INSTRUCTIONS BEFORE COMPLETING FORM

1. REPORT NUMBER: Technical report no. 4	2. GOVT ACCESSION NO.
3. RECIPIENT'S CATALOG NUMBER	
4. TITLE (and Subtitle): Raman and Infrared Spectroscopy of Aqueous Corrosion Films on Lead	5. TYPE OF REPORT & PERIOD COVERED: Technical 1978
	6. PERFORMING ORG. REPORT NUMBER
7. AUTHOR(s): R. Heidersbach, C. Brown, R. Thibeau and A. Goldfarb	8. CONTRACT OR GRANT NUMBER(s): N00014-76-c-0889
9. PERFORMING ORGANIZATION NAME AND ADDRESS: Department of Ocean Engineering, University of Rhode Island, Kingston, Rhode Island 02881	10. PROGRAM ELEMENT, PROJECT, TASK AREA & WORK UNIT NUMBERS
11. CONTROLLING OFFICE NAME AND ADDRESS: Office of Naval Research, Department of the Navy, Arlington, Virginia 22217	12. REPORT DATE: August 1978
	13. NUMBER OF PAGES: seventy-two (72)
14. MONITORING AGENCY NAME & ADDRESS (if different from Controlling Office)	15. SECURITY CLASS. (of this report): unclassified
	15a. DECLASSIFICATION/DOWNGRADING SCHEDULE

16. DISTRIBUTION STATEMENT (of this Report)

This document has been approved for public release and sale; its distribution is unlimited.

17. DISTRIBUTION STATEMENT (of the abstract entered in Block 20, if different from Report)

18. SUPPLEMENTARY NOTES

19. KEY WORDS (Continue on reverse side if necessary and identify by block number)

Passivity; surface chemistry; lead; water; corrosion; chloride

20. ABSTRACT (Continue on reverse side if necessary and identify by block number)

The use of Raman and infrared spectroscopy to analyze surface films on metals is described. Surface films formed on lead by reaction with aqueous buffer solutions were examined. The composition of each film was determined by Raman spectroscopy while the sample was in the solution. Multiple reflection infrared spectra of dry samples confirmed the Raman results.

The Pourbaix diagrams for lead in water with and without chloride were calculated and potentiostatic exposures were conducted to see if the com-

cont.....

DD FORM 1 JAN 73 1473 EDITION OF 1 NOV 65 IS OBSOLETE

SECURITY CLASSIFICATION OF THIS PAGE (When Data Entered)

20. Abstract (cont.)

pounds correspond to those predicted in the diagram. Tetragonal PbO was found to occur over a much greater range of potentials than thermodynamic stability would indicate. Several differences due to the presence of chlorides were noted.

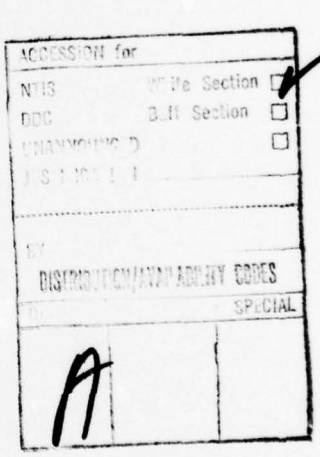

This report consists of the manuscripts of two papers which have been submitted for publication in the Journal of the Electrochemical Society.

INFRARED AND RAMAN SPECTROSCOPY OF AQUEOUS CORROSION FILMS ON LEAD

RICHARD J. THIBEAU AND CHRIS W. BROWN
DEPARTMENT OF CHEMISTRY

ARNON Z. GOLDFARB AND ROBERT H. HEIDERSBACH*
DEPARTMENT OF OCEAN ENGINEERING

UNIVERSITY OF RHODE ISLAND
KINGSTON, RHODE ISLAND 02881

SUBMITTED TO

JOURNAL OF THE ELECTROCHEMICAL SOCIETY

*Electrochemical Society Active Member

ABSTRACT

The use of Raman and infrared spectroscopy to analyze surface films on metals is described. Surface films formed on lead by reaction with aqueous buffer solutions were examined. The composition of each film was determined by Raman spectroscopy while the sample was in the solution. Multiple reflection infrared spectra of dry samples confirmed the Raman results.

The Pourbaix diagram for lead in water was calculated and potentiostatic exposures were conducted to see if the compounds correspond to those predicted in the diagram. Tetragonal PbO was found to occur over a much greater range of potentials than thermodynamic stability would indicate.

INTRODUCTION

Passive films play an important role in corrosion and other electrochemical phenomena. Passive film studies frequently emphasize either the kinetics of film growth, breakdown and repair or else they emphasize the structure and composition of the film. A number of techniques have been developed for both purposes.

This investigation was aimed at demonstrating the use of infrared (IR) and Raman spectroscopy for studying passive films formed on lead. The advantages of these techniques for studies of this type are also discussed.

Surface Analysis Techniques: A number of techniques are available for the study of passive film composition and structure. Recent reviews by Vermilyea (1) and Leidheiser (2) discuss most of the important surface analysis techniques available for use in studying passive films. Table 1 summarizes the techniques used in corrosion studies.

The ideal surface analysis technique would be able to provide structural information, in situ, on a variety of substrates. It should require no vacuum, work on amorphous as well as crystalline films, and be confirmable by other techniques. It should cover the entire atomic spectrum and not be limited, as is the case with Mossbauer spectroscopy, to certain elements (4). It is clear that Raman spectroscopy, with its unique capability for in situ analysis of passive films as they form in aqueous media, has several important advantages over other surface analysis techniques. The combination of infrared and Raman spectroscopy offers structural

analysis possibilities which cannot be met by any other surface analysis techniques.

VIBRATIONAL SPECTROSCOPY

Infrared and Raman Spectroscopy: Infrared and Raman spectroscopy are two similar structural analysis techniques. They are complementary in that one technique will often be highly sensitive to certain structures at the same time that the other technique will provide little, or no, information. For this reason they are usually used together, and the term vibrational spectroscopy is used to cover both techniques.

The optical schematic of a typical infrared spectrometer used for surface studies is shown in Figure 1. Instruments of this type for use in corrosion studies were first described by Hannah (5), and subsequently have been used by Poling (6, 7), Mertens (8) and others. Light from a single infrared source is split and directed along two parallel light paths. The sample(s) of interest are inserted into one light path (m_3 in Figure 1), and the combination infrared reflection-absorption spectrum obtained from the sample is compared with the spectrum obtained in the reference beam, which is identical to the sample path in all aspects except the identity of the sample mirror. Comparison of the sample and reference beams eliminates source and light path artifacts from the spectrum (9). It is beyond the purposes of this paper to discuss the reflection-absorption nature of the infrared spectra obtained using this technique. Detailed discussions of this are available (10-12).

To understand vibrational spectroscopy, let us first consider the vibrational energy levels of a diatomic molecule. The lowest two vibrational energy levels with v = 0 and v = 1 (where v is the vibrational quantum number) are shown in Figure 2. The energy of each state is proportional to the frequency of vibration, i.e.,

$$\varepsilon_v = (v + 1/2)\ h\nu_i c$$

where h is Plank's constant, c the speed of light, and ν the vibrational frequency. Molecules can absorb light by going from the lower to the higher level, or they can emit light by going from the higher to the lower. The energy corresponding to the absorption of light is given by

$$\Delta\varepsilon = \varepsilon_{v=1} - \varepsilon_{v=0} = h\nu_i c$$

A typical transition for a diatomic molecule corresponds to $\sim$ 2,000 cm^{-1}, and the absorption appears in the infrared range of the electromagnetic spectrum.

An infrared absorption spectrum is obtained by passing infrared radiation through a partially transmitting sample. If the sample consists of diatomic molecules having dipole moments, some of the light will be absorbed at the resonance frequency of the molecules, i.e., the frequency corresponding to a transition between the v = 0 and v = 1 levels. Non-linear polyatomic molecules have 3N - 6 (where N = the number of atoms) excited levels with v = 1, i.e., there are 3N - 6 different vibrations. In an infrared spectrum of a polyatomic molecule there may not be 3N - 6 absorption bands, since all of the excited states may not be accessible through absorption

of infrared radiation. In summary, infrared spectra of liquids and solids are due to transitions between vibrational energy levels.

The optical schematic of a modern Raman spectrometer is shown in Figure 3. The spectrometer consists of a laser, a sample compartment, an optical manochromater, and a detection system. The laser acts as a source of monochromatic light which strikes the sample. Most of the incident light is reflected from the sample surface and undergoes no change in wavelength. However, some of the incident light interacts with the surface, loses some of its energy, and causes emission of light at wavelengths different than the incident radiation. It is this emitted light which is measured in Raman spectroscopy.

The transitions responsible for Raman scattering are shown in Figure 4. Consider a molecule in the ground (v = 0) vibrational state. The incident radiation in the visible range (e.g., ν_o = 20,000 cm^{-1}) excites the molecule to a pseudo energy level by inducing a temporary dipole in the molecule. In a short time period ($\sim 10^{-14}$ sec) the molecule emits a photon at the same frequency (Rayleigh scattering) and returns to the ground state, or it emits a photon at a lower frequency and returns to a higher vibrational level, e.g., v = 1. In the latter case, the energy of the photon will correspond to a frequency $\nu_o - \nu_i$; this type of transition is referred to as Stokes Raman scattering.

There is a Boltzmann distribution of molecules at all possible vibrational energy levels. Thus, even at room tem-

perature there are molecules in the v = 1 level. These can also be excited by the incident radiation to a psuedo level. These molecules can then return to the same level and emit a photon of ν_o, or they can return to v = 0 and emit a photon of $\nu_o + \nu_i$. These latter transitions are also Raman, and are referred to as anti-Stokes Raman scattering.

A typical Raman spectrum of a diatomic molecule is shown in the bottom of Figure 4. The intensity of the anti-Stokes Raman bands depends upon the magnitude of ν_i, i.e., the greater ν_i, the smaller the number of molecules in the level (Boltzmann distribution) and the smaller the intensity of the transition. Thus, in conventional Raman spectroscopy we measure only the Stokes transitions and only the left half of the spectrum is used. Furthermore, it is conventional to plot the frequency difference, i.e., $\nu_o - (\nu_o - \nu_i) = \nu_i$, or the frequency corresponding to the differences between vibrational levels. For polyatomic molecules, Raman transitions to some or all of the possible 3N - 6 vibrational levels can take place.

For a Raman transition to occur, the geometry of the molecule in the excited state must be such that a change in polarizability has taken place, i.e., the electron density about the molecule must be distorted by the transition. For an absorption of infrared radiation to occur, the geometry of the molecule in the excited state must be such that a change in the dipole moment has taken place. Thus, both Raman and infrared absorption spectra provide data on vibrational transitions which in turn provide information on the bonding and the structure of the molecule. However, the two processes are entirely different,

and one may occur without the other. Generally, they provide complementary information, and both spectra are needed to completely understand the vibrational properties of chemical species.

Every molecule has its own characteristic infrared and Raman spectrum which can be used to identify the molecule (exceptions are homonuclear diatomic molecules which do not absorb infrared radiation). The primary use of these techniques has been in identification. The spectrum of an unknown chemical can be identified by comparing its infrared or Raman spectral "fingerprint" to those of known chemicals. It is this method that we have used to identify the composition of films on the surface of metals, i.e., we compare spectra from surface films with spectra of known chemicals.

Pourbaix Diagrams: Potential-pH diagrams (Pourbaix diagrams) are available for a wide variety of metals (13), and they have found wide application in corrosion research (14, 15). The Pourbaix diagram of lead (13) was used as a basis for choosing exposure conditions for forming passive films on lead surfaces which were subsequently analyzed by Raman and infrared spectroscopy in this study.

EXPERIMENTAL

Raman spectra were recorded with a Spex Industries Model 1401 double monochromator using a photon counting detection system. A simplified optical schematic of a spectrometer of this type is shown in Figure 3. A Coherent Radiation Laboratories Model CR-3 argon ion laser is located beneath the monochromator and the laser beam is directed by a mirror to the

bottom of the sample cell. Some of the light scattered by the sample is collected by the lens (L), positioned 90° from the vertical laser beam, and is focussed onto the entrance slits of the monochromator. Light passing through the slits is collimated by a mirror and dispersed by the first grating. The light, spread out according to frequency, is then directed by a second collimating mirror and a plane mirror to the intermediate slits. The narrow frequency band of light which has passed through the first monochromator then passes through a second identical monochromator, to maximize rejection of stray light, and reaches the detector, a photomultiplier tube. Each photon reaching the photomultiplier is converted to an electrical pulse which is amplified and counted. The number of counts (number of photons) per selected time interval is converted to an analog signal which drives the pen on a strip chart recorder. A frequency range is scanned by turning the two gratings in the monochromator simultaneously so the frequency of light reaching the detector is changed. The Raman spectrum recorded is thus a plot of light intensity versus frequency difference from the excitation frequency.

The electrochemical cell shown in Figure 5 is used in the sample compartment of the spectrometer to allow Raman spectra to be recorded while the sample is undergoing oxidation in an aqueous solution. The cell is designed for potentiostatic exposures of fairly large samples. The working electrode is a flat 2.8 x 5.7 cm rectangular sample held in a Teflon sample

holder. The auxiliary electrode is platinum mesh and the potential is maintained relative to a saturated calomel electrode by a potentiostat. The sample is held close to the bottom and side of the cylindrical glass cell and at an angle of 20^{o} from vertical so that it is in the optimum position for observation of Raman spectra. The angles between the sample surface and the incident beam and between the surface and the axis of the collection optics are important in optimizing the efficiency of collecting Raman scattered light (16). The angles are chosen so that the electric vector of the incident beam may interact most strongly with the film and Raman scattered light may reflect off of the surface and interfere constructively with the scattered light which is not reflected.

The sample size (2.8 x 5.7 cm) was selected so that the sample, after in situ examination by Raman spectroscopy, can be placed in the holder of a Wilks Scientific Corporation Model 9 multiple specular reflection attachment for infrared reflection-absorption analysis. An optical schematic of the reflection attachments in the Perkin-Elmer Model 521 infrared spectrophotometer is shown in Figure 1. Two multiple reflection attachments are used in the spectrophotometer; one in the sample beam holding the oxidized metal sample, and one in the reference beam holding an aluminum mirror.

Each time the infrared beam reflects off of the sample surface some radiation is absorbed by the surface film at frequencies of infrared absorption bands. Some light is also

lost at all frequencies with each reflection so the mirrors are adjusted to provide the optimum angle of incidence (65^{o} - 88^{o}, depending on film thickness) and the optimum number of reflections (1-3) for recording the spectrum of a film on a lead substrate. After the sample and reference beams are combined in the monochromator portion of the instrument, the light must pass through a polarizer which transmits only that light with its electric vector in the plane parallel to the plane of incidence with the sample surface. Only the parallel polarized light will interact with a thin film (11) so the extra light not in this plane, and containing no information, is filtered out to increase the sensitivity of the instrument.

Lead foil (Alfa Products, Inc., Danvers, Massachusetts), 1 mm thick and 99.9995% pure, was cleaned by immersion in warm, concentrated ammonium acetate solution for five minutes and rinsed with distilled water before being placed in solution in the electrochemical cell. The solution was purged of reactive dissolved gases by bubbling dry nitrogen through it for an hour before and throughout the period of sample exposure. For a few exposures, the lead sample was not connected to the potentiostat but was allowed to react at its equilibrium potential. For other exposures, the potentiostat was turned on immediately after placing the sample in solution, and it maintained the potential at a constant value throughout periods of exposure which ranged from 6 minutes to 24 hours.

Some exposures were conducted on lead films which were vapor deposited onto gold substrates on glass microscope slides. These samples, similar to those used by Poling in his infrared studies of high temperature oxidation of iron and copper (6), allowed the lead to be completely oxidized leaving a nonreacted gold mirror substrate.

RESULTS AND DISCUSSION

Spectra: A lead sample was immersed in 2.3 m hydrobromic acid and allowed to corrode freely (no connection to the potentiostat). After 8 days the in situ Raman spectrum of the surface shown in Figure 6 was recorded. The spectrum of the gray surface layer clearly indicates that it consists of $PbBr_2$. The six strongest bands in the spectrum of pure $PbBr_2$ are present in the spectrum of the film. Furthermore, the band shapes and frequencies in the spectra of the film and the powder are identical.

The sample was allowed to continue reacting undisturbed in the solution and white needle-like crystals formed on the surface. After immersion for 34 days, the sample was removed and dried. The white crystals were scraped off and ground into powder. The spectrum of the resulting powder was identical to that of the surface film. It is clear that the Raman spectrum of a thick film is identical to that of a bulk sample. Possibly a spectrum of an extremely thin film might differ due to changes in the bonds because the surface compound is bound to the underlying metal, but for relatively thick films (hundreds or thousands of angstroms) the spectra are the same as that of a powder.

At this point is should also be pointed out that the films analyzed in this investigation were surface reaction products. No attempt was made to separate precipitated deposits, such as those discussed above, from adherent conversion products which may have acted as passive films and altered metal-environment reaction kinetics.

Analysis of surface films by infrared spectroscopy gives somewhat different results. While the entire range of vibrational bands, from lattice modes at 20 cm^{-1} to overtones beyond 6000 cm^{-1}, are easily observed with a Raman spectrometer, normally two different instruments are required to scan that range in the infrared. For this study, infrared spectra were obtained in the region 1500-250 cm^{-1}. The low frequency bands of a compound like lead bromide could not be observed. Nearly all infrared spectra found in the literature are transmission spectra, observations of the amount of light passing through a partially absorbing sample. By combining absorption with reflection at the surface film-metal interface, the resulting spectrum has a different appearance from a pure absorption spectrum. An infrared reflection-absorption spectrum results from changes in the extinction coefficient and the index of refraction, both of which can change radically in the vicinity of an absorption frequency, whereas a transmission spectrum is due to changes in extinction coefficient alone. The result, as demonstrated in Figure 7, is that a reflection-absorption spectrum usually has bands of slightly different shape and frequency from a transmission spectrum. The magnitude of the differences depends on such variables as angle of incidence of

the infrared beam, film thickness, and number of reflections used. Because of the changeability of spectra as instrumental conditions are changed, identification of compounds with infrared reflection-absorption alone is sometimes difficult but, combined with Raman spectra, identification can be very accurate.

Some compounds have vibrational transitions which are much stronger in the infrared than in Raman, and some have vibrations which are much stronger in Raman spectra. The basic lead carbonate, $(PbCO_3)_2 \cdot Pb(OH)_2$, on the lead surface that produced the strong infrared spectrum of Figure 7 produced only a weak Raman band at 1050 cm^{-1} to indicate the presence of carbonate. Although $(PbCO_3)_2 \cdot Pb(OH)_2$ can give the Raman spectrum shown in Figure 8, it was necessary to use the complementary technique, infrared absorption, to specify which carbonate compound was present.

Water is a strong infrared absorber so samples must be dried before a spectrum can be observed. This is not the case with Raman spectroscopy; water poses little problem in obtaining a Raman spectrum. For potentiostatically exposed samples, Raman spectra were recorded with the sample in the solution with a potential applied. After obtaining a spectrum the sample was removed from the electrochemical cell, washed with distilled water, and dried at room temperature. The dry sample was then returned to the spectrometer sample compartment and another Raman spectrum recorded. This was done to identify any changes that might occur in the surface film upon drying. In the pre-

sent investigation no significant differences between in situ and dry sample Raman spectra were found. Spectra obtained under both conditions are very similar as demonstrated in Figure 9. Both spectra contain the three strongest bands of tetragonal PbO, enough to conclusively identify the compound as the surface species present. After removal from the cell and drying of the sample, the spectrum is slightly stronger. In this investigation the intensity of the Raman spectra recorded with samples in solution in the electrochemical cell was approximately half the spectral intensity of dry samples. The reasons for the decrease in intensity are scattering and reflection from the solution and sides of the cell and the difficulty of focussing light scattered in the cell onto the monochromator entrance.

Figure 10 shows the Raman spectrum of orthorhombic PbO. The thickness of the film that produced the spectrum was measured at 1600 Å using a Taylstep-1 stylus instrument. From the PbO spectra obtained in this investigation for vapor-deposited samples, it is estimated that a minimum film thickness of approximately 200 Å is necessary to obtain usable spectra using the infrared and Raman instruments employed. Other oxides should have different minimum detectable thicknesses. Other researchers have reported infrared spectra from thinner films formed on non-lead substrates (5-8).

Single spectrometer scans were used to record the spectra recorded in this investigation. Signal averaging of multiple scans should increase the signal to noise ratio and reduce the minimum detectable thicknesses (17).

The Lead-Water Pourbaix Diagram: Most available potential-pH (Pourbaix) diagrams are based on the same type of thermodynamic calculations employed by Pourbaix in compiling his original atlas (13). Several experimental Pourbaix diagrams have appeared (14,15,18-21) and these are normally based on electrochemical polarization techniques which emphasize electrode kinetics.

Vibrational spectroscopy seems uniquely suited to analyze, in situ, films formed on metals under passivating conditions as predicted by Pourbaix diagrams. In this manner, experimental determinations of the composition of films formed in the passive region of a Pourbaix diagram should be possible.

The Pourbaix diagram of lead was chosen to test this hypothesis. Lead was chosen because its high atomic weight means that lead compounds should be relatively strong Raman scatterers (22). The lead diagram also contains a number of different insoluble species and is similar to iron, the most important structural metal, in many respects (13). A report of similar attempts to verify some portions of the lead Pourbaix diagram using Raman spectroscopy was published during the course of this investigation (22).

The lead-water equilibrium diagram published by Pourbaix is shown in Figure 11. Initial attempts to verify this diagram using infrared and Raman spectroscopy led to a number of discrepancies between predicted and experimentally determined passive species. Recalculation of the Pb-H_2O equilibria using the most recent thermodynamic data from the National Bureau of Standards (24) resulted in the diagram of Figure 12. It was

hoped that fewer differences between predicted and observed species would be noted when this new data was used. Unfortunately, the discrepancies still remain after recalculation; possible reasons for these discrepancies are discussed later in this report. The free energies of formation for the species in question in Figures 11 and 12 are listed in Table II.

Figure 12 was used, in conjunction with potentiodynamic polarization curves run in the solutions of interest, to identify potential-pH combinations to be used to form passive films for spectroscopic investigation. Table III lists the electrolytes used. They are similar to those used by Pourbaix, Verink, and coworkers at the University of Florida (25) and have been used in other electrochemical studies in these laboratories (20). The exposures performed in this investigation are summarized in Table IV.

The results in the immunity (low potential) region of the Pourbaix diagram agree with the thermodynamic predictions summarized in Figure 12 except for the appearance of basic lead carbonate at some potentials in pH 10. Spectra of tetragonal PbO were observed in regions where PbO, Pb_3O_4, Pb_2O_3, and PbO_2 were predicted by thermodynamics. At lower potentials the sample surfaces remained shiny, oxidation was relatively slow, and the oxide films were apparently thin. At higher potentials the metallic surface quickly became black. The black lead oxide has been previously described as PbO with a thin outer surface film of elemental lead (26). At the slower rates of oxidation occurring at lower potentials, the film did not become black.

The formation of tetragonal PbO under conditions where other oxides are predicted to be stable cannot be adequately explained. It must be noted, however, that, if PbO_2 were formed, it could probably not be detected using infrared and Raman spectroscopy. Lead dioxide has been reported to have no infrared absorption bands in the region 1500-250 cm^{-1} (27), and no Raman spectra were observed from bulk samples of reagent grade PbO_2 (28).

Spectra have been obtained for orthorhombic PbO and Pb_3O_4 and are reported elsewhere (27-30). The lack of observation of these species during the electrochemical exposures of the investigation may be due to errors in the theoretical Pourbaix diagram (Figures 12 and 13). Another possibility is the presence of insufficient amounts of these compounds to be detectable by the instrumentation used. The possibility of a multilayered film with an outer layer, which is detectable spectroscopically, masking an inner film must also be considered (10).

CONCLUSIONS

Infrared and Raman spectroscopy can be used to identify surface films formed on electrolytes in corrosive environments. Raman spectra can be obtained in situ in aqueous environments. There are only slight differences in intensity between in situ Raman spectra and those recorded on dry samples. Multiple reflection infrared spectroscopy complements in situ Raman spectroscopy.

Surface films identified on lead samples using infrared and Raman spectroscopy differed from those predicted by thermo-

dynamics. Differences may be due to experimental limitations or may indicate deficiencies in thermodynamic prediction techniques such as anion effects which are not considered in the calculations for Figures 11 and 12.

ACKNOWLEDGEMENT

This work was supported by the Department of the Navy, Office of Naval Research, under contract N00014-76-C-0889.

REFERENCES

1. D.A. Vermilyea, Physics Today, September 1976, 23.
2. H. Leidheiser, Proceedings; 4th International Conference on Passivity, Airlie, VA, October 1977.
3. Lieng-Huang Lee, Characterization of Metal and Polymer Surfaces, L.H. Lee, ed., Academic Press, NY, 1977, Vol. 1, pg. 1.
4. U. Gonser, Mossbauer Spectroscopy, Springer-Verlag, Berlin, 1975.
5. R.W. Hannah, Appl. Spectroscopy, 17, 23 (1963).
6. G.W. Poling, J. Electrochem. Soc., 116, 958 (1969).
7. G.W. Poling, J. Colloid Interface Sci., 34, 365 (1970).
8. F.P. Mertens, Surface Sci., 71, 161 (1978).
9. M.L. Hair, Infrared Spectroscopy in Surface Chemistry, Marcel Dekker, NY, 1967.
10. A.Z. Goldfarb, M.S. Thesis, University of Rhode Island, (1978).
11. R.G. Greenler, J. Chem. Phys., 44, 310 (1966).
12. R.G. Greenler, J. Chem. Phys., 50, 1963 (1968).
13. M. Pourbaix, Atlas of Electrochemical Equilibria in Aqueous Solutions, NACE, Houston, 1969.
14. K.D. Efrid, Corrosion, 31, 77 (1975).
15. E.D. Verink and T. Lee, Proceedings of the Third International Conference on Marine Corrosion and Fouling, Gaithersburg, MD, 1972.
16. R.G. Greenler and T.L. Slager, Spectrochim. Acta, 29A, 193 (1972).
17. C.H. Warren and L. Ramaley, Appl. Opt., 12, 1976 (1973).
18. E.D. Verink and R.H. Heidersbach, Localized Corrosion-Cause of Metal Failure, ASTM STP 516, American Society for Testing and Materials, 1972, p. 303.
19. P. Parrish, M.S. Thesis, University of Florida (1970).
20. R. Turcotte, M.S. Thesis, University of Rhode Island (1977).

21. E.D. Verink and M. Pourbaix, Corrosion, 27, 12 (1971).

22. N. Colthup, L. Daly, and S. Wiberley, Introduction to Infrared and Raman Spectroscopy, second ed., Academic Press, NY, 1975.

23. E.S. Reid, R.P. Cooney, P.J. Hendra, and M. Fleischmann, J. Electroanal. Chem., 80, 405 (1977).

24. D.D. Wagman, W.H. Evans, V.B. Parker, I. Halow, S.M. Bailey, and R.H. Schumm, NBS Technical Note 270-3, U.S. Government Printing Office, 1975.

25. R.L. Cusumano, M.S. Thesis, University of Florida (1971).

26. E.W. Abel, Comprehensive Inorganic Chemistry, J.C. Bailar, H.J. Emeleus, R. Nyholm, and A.F. Trotman-Dickenson, eds., Pergamon, 1973, vol. 2, p. 119.

27. N.T. McDevitt and W.L. Baun, Spectrochim. Acta, 20, 799 (1964).

28. R.J. Thibeau, Ph.D. Thesis, University of Rhode Island (1978).

29. J.D. Donaldson, M.T. Donoghue, and S.D. Ross, Spectrochim. Acta, 30A, 1967 (1974).

30. D.M. Adams and D.C. Stevens, J.C.S. Dalton, 1977, 1096.

FIGURE CAPTIONS

Figure 1. Optical schematic of the infrared reflection-absorption setup used. S is the infrared source, reflecting surfaces are labelled m, and the sample is at position m_3.

Figure 2. Vibrational energy levels of a diatomic molecule.

Figure 3. Schematic drawing of a laser Raman spectrometer. Mirrors are labelled M, gratings, G, and slits, S.

Figure 4. Energy level diagram for a typical vibrational Raman transition and the Raman spectrum resulting from such a transition.

Figure 5. Drawing of the electrochemical cell used for in situ Raman spectroscopy.

Figure 6. Raman spectra of a) the surface of lead foil immersed in deaerated 2.3M HBr solution for 8 days, b) $PbBr_2$ powder from crystals formed on lead in 2.3 M HBr after 34 days, c) reagent grade $PbBr_2$ powder.

Figure 7. a) Infrared reflection-absorption spectrum of a lead sample after exposure in pH 10 solution at -0.42V vs. NHE for 24 hours, b) transmission infrared spectrum of $(PbCO_3)\cdot Pb(OH)_2$ in a KBr pellet.

Figure 8. Raman spectrum of reagent $(PbCO_3)_2\cdot Pb(OH)_2$ in a KBr pellet.

Figure 9. Raman spectra of a lead surface in pH 7 solution at + 0.06 V vs. NHE after 2 hr. 50 min. exposure and of the same sample after washing with distilled water and drying.

Figure 10. Raman spectrum of a 1600 Å thick film of orthorhombic PbO made from a vacuum deposited lead sample. Grating ghost marked with an asterisk.

Figure 11. Pb-H_2O Pourbaix diagram, ref. 13.

Figure 12. Calculated Pb-H_2O Pourbaix diagram using the most recent NBS data (24). Experimental results, 0 = tetragonal PbO, i = apparent immunity, no spectrum observed, C = basic lead carbonate.

TABLE I. CHARACTERISTICS OF SURFACE ANALYTICAL TECHNIQUES

ANALYTICAL METHOD	TYPICAL BACKGROUND PRESSURE (TORR)	ANALYSIS IN AQUEOUS SOLUTION	MIN. FILM THICKNESS OBSERVED (Å)	INFORMATION OBTAINED
Raman spectroscopy	760	Yes	50[16]	compound identification
Infrared spectroscopy	760	No	10[5]	compound identification
X-ray diffraction	760	No	500	compound identification
Ellipsometry[2]	760	Yes	10	film thickness
Low energy electron diffraction[2] (LEED)	10^{-10}	No	monolayer	compound identification
Auger electron spectroscopy[2] (AES)	10^{-9}-10^{-10}	No	monolayer	elemental composition
Secondary ion mass spectrometry[2] (SIMS)	10^{-10}	No	monolayer	elemental composition
Electron microprobe analyzer[2]	10^{-5}-10^{-10}	No	200	elemental composition
Scanning electron microscope[2] (SEM)	10^{-4} 10^{-9}	No	50	surface topography
Electron Spectroscopy for chemical analysis[2] (ESCA)	10^{-7} 10^{-10}	No	5	elemental composition, electronic states

TABLE II. FREE ENERGY DATA USED TO CALCULATE THE Pb-H_2O POURBAIX DIAGRAM

ΔG_f^o (cal/mole)

	NBS (24)	Pourbaix (13)
Pb^{++}	-5,830	-5,810
PbO (orthorhombic)	-44,910	-45,050
PbO (tetragonal)	-45,160	-45,250
PbO_2 (orthorhombic)	-51,950	-52,340
Pb_3O_4	-143,700	-147,600

TABLE III. ELECTROLYTE SOLUTIONS USED IN THIS INVESTIGATION

Composition	pH
2.3 M HBr	
0.063 M KH_2PO_4, 0.037 M NaOH	7.0
0.041 M $NaHCO_3$, 0.018 M NaOH	10.0

TABLE IV. CONTROLLED POTENTIAL-pH EXPOSURES OF LEAD IN AQUEOUS SOLUTIONS

SOLUTION pH	POTENTIAL V VS. NHE	DURATION OF EXPOSURE	CURRENT DENSITY, $\mu a/cm^2$ (a)	SURFACE SPECIES PREDICTED	SURFACE SPECIES EXPER. OBSERVED
7	-0.62	17 hr.	1.7 (b)	Pb	none
7	-0.62	19 hr.	1.2 (b)	Pb	none
7	-0.16	20 hr.	6.3	Pb	none
7	-0.12	18 hr.	61	PbO	Tetrogonal PbO
7	+0.06	2.8 hr.	112	PbO	Tetragonal PbO
7	+0.48	21 hr.		PbO	Tetragonal PbO
7	+0.58	3 hr.		PbO	Tetragonal PbO
7	+0.67	2 hr.	310	Pb_3O_4	Tetragonal PbO
7	+0.74	23.5 hr.	397	Pb_2O_3	Tetragonal PbO
7	+1.08	1.5 hr.	310	PbO_2	Tetragonal PbO
7	+1.08	18 hr.	294	PbO_2	Tetragonal PbO
10	-0.80	20.5 hr.	139 (b)	Pb	none
10	-0.42	18 hr.	24	Pb	$(PbCO_3)_2 \cdot Pb(OH)_2$
10	-0.28	4 hr.		Pb	Tetragonal PbO and $(PbCO_3)_2 \cdot Pb(OH)_2$
10	-0.26	21 hr.	14.3	PbO	Tetragonal PbO
10	-0.03	17 hr.	46	PbO	Tetragonal PbO
10	+0.02	23 hr.		PbO	Tetragonal PbO
10	+0.24	17 hr.	54	PbO	Tetragonal PbO
10	+0.34	2 hr.	455	PbO	Tetragonal PbO
10	+0.46	2.5 hr.	210	Pb_3O_4	Tetragonal PbO
10	+0.75	0.75 hr.		PbO_2	Tetragonal PbO
10	+0.75	18 hr.		PbO_2	Tetragonal PbO
10	+0.84	1.5 hr.	115	PbO_2	Tetragonal PbO

TABLE IV. (CONT.)

10	+0.94	6 min.	175	PbO_2	Tetragonal PbO
10	+0.94	17.5 hr.	91	PbO_2	Tetragonal PbO
10	+1.24	17 hr.	1200	PbO_2	Tetragonal PbO

(a) final or steady current

(b) current flow in reducing direction

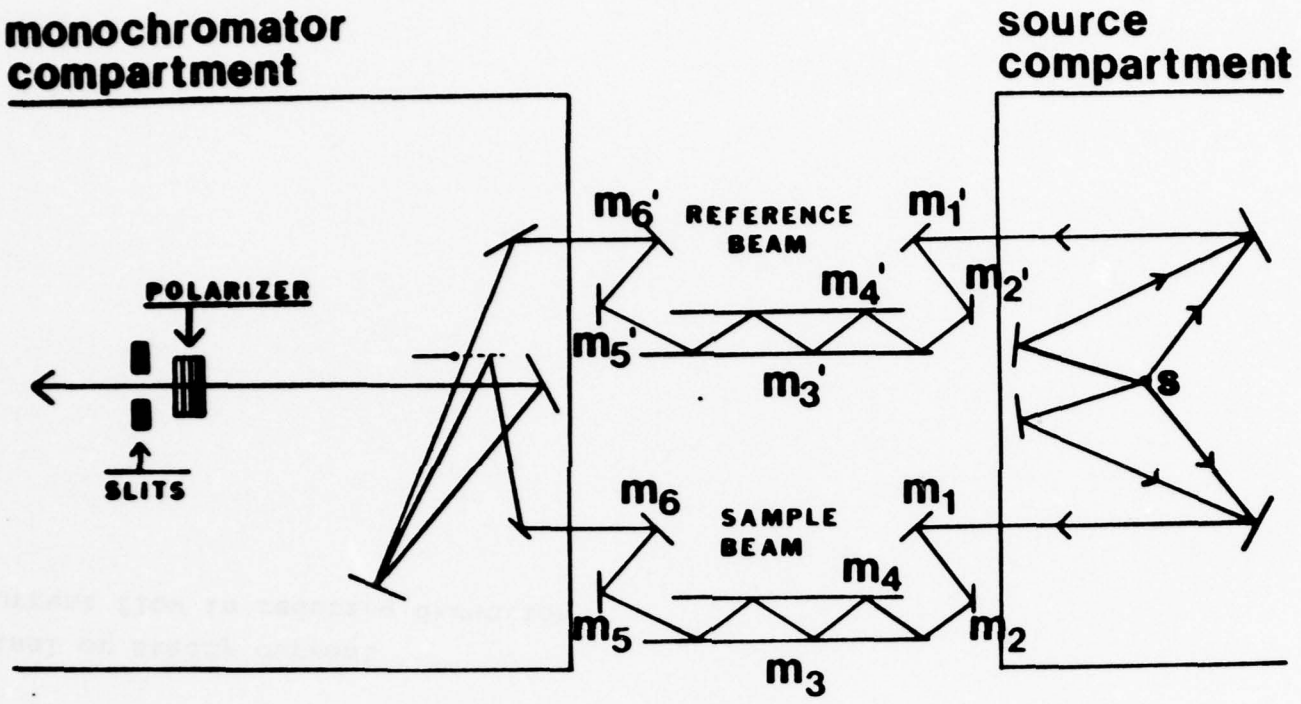
monochromator compartment
source compartment
POLARIZER
SLITS
REFERENCE BEAM
SAMPLE BEAM
m6'
m1'
m4'
m2'
m5'
m3'
S
m6
m1
m4
m5
m2
m3

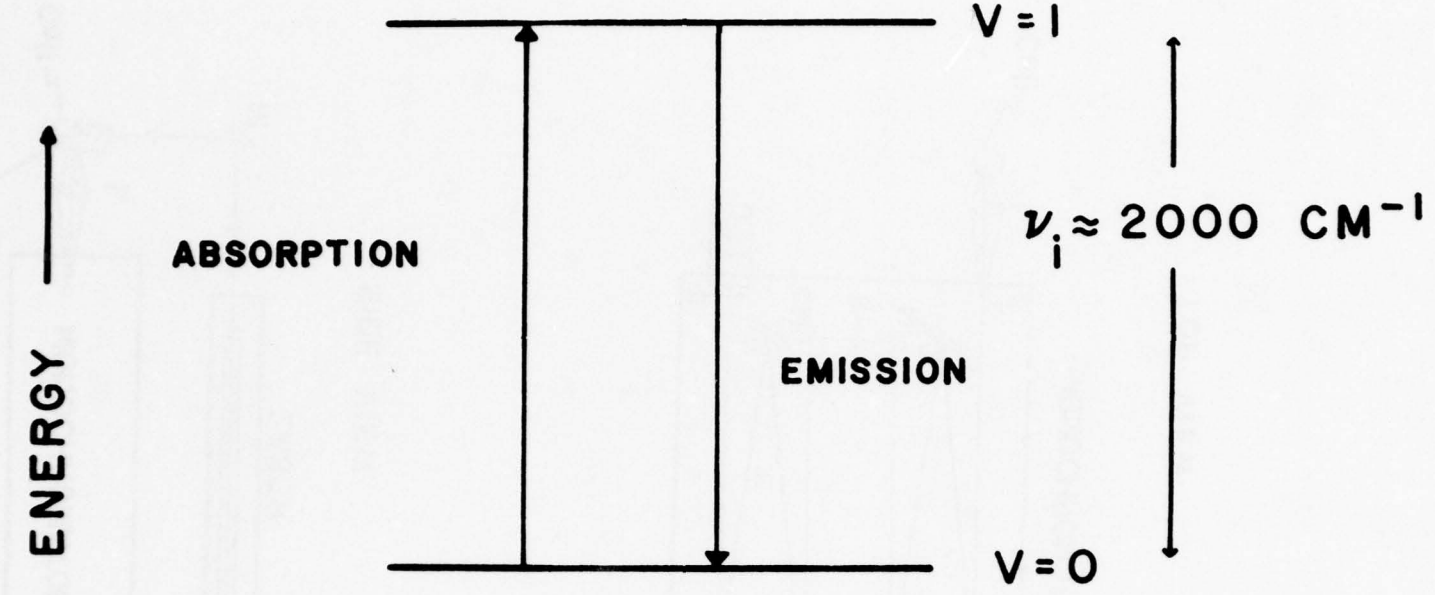
V = 1
ENERGY
ABSORPTION
EMISSION
$\nu_i \approx 2000$ CM^{-1}
V = 0

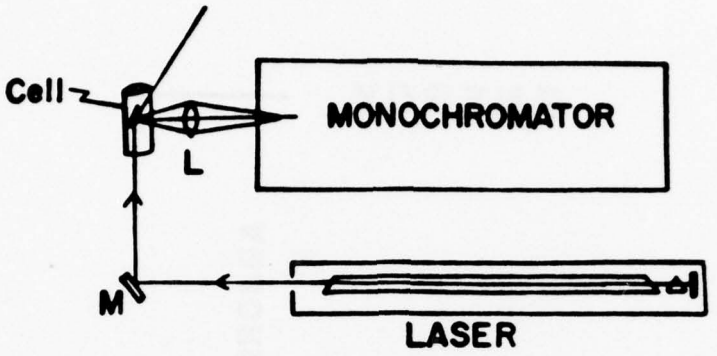

SIDE VIEW

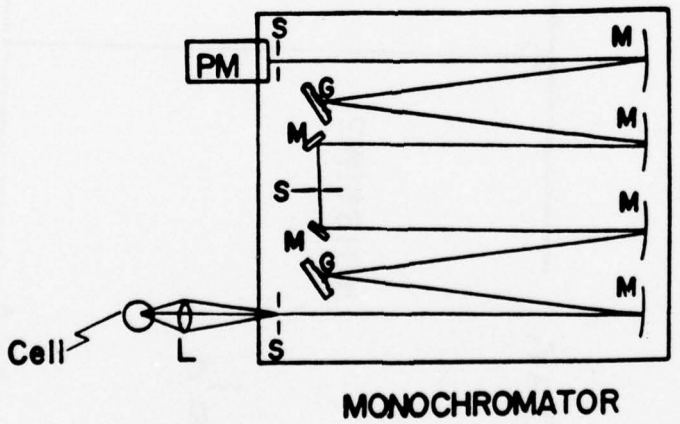

TOP VIEW

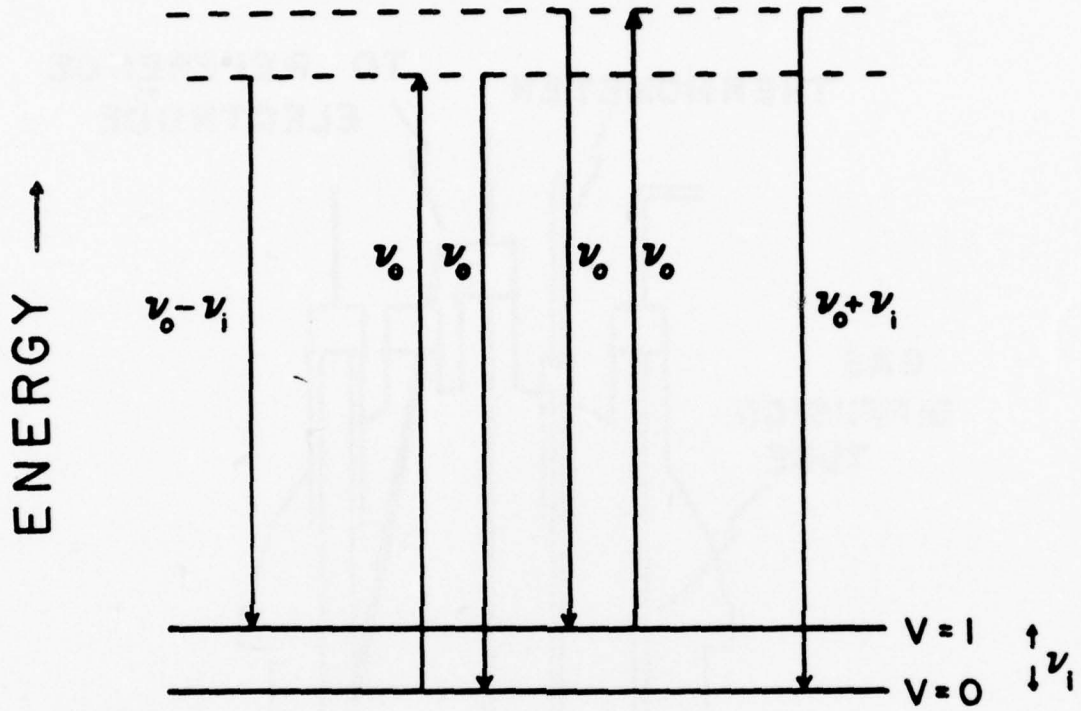
ENERGY
$\nu_0 - \nu_i$
ν_0
ν_0
ν_0
ν_0
$\nu_0 + \nu_i$
V=1
V=0
ν_i

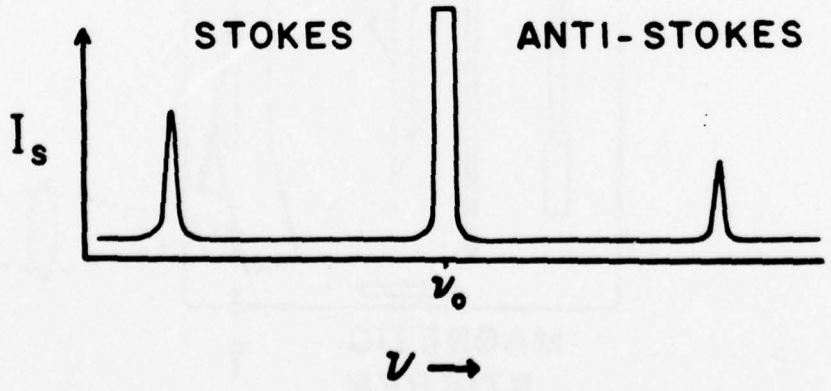
STOKES
ANTI-STOKES
I_s
ν_0
ν

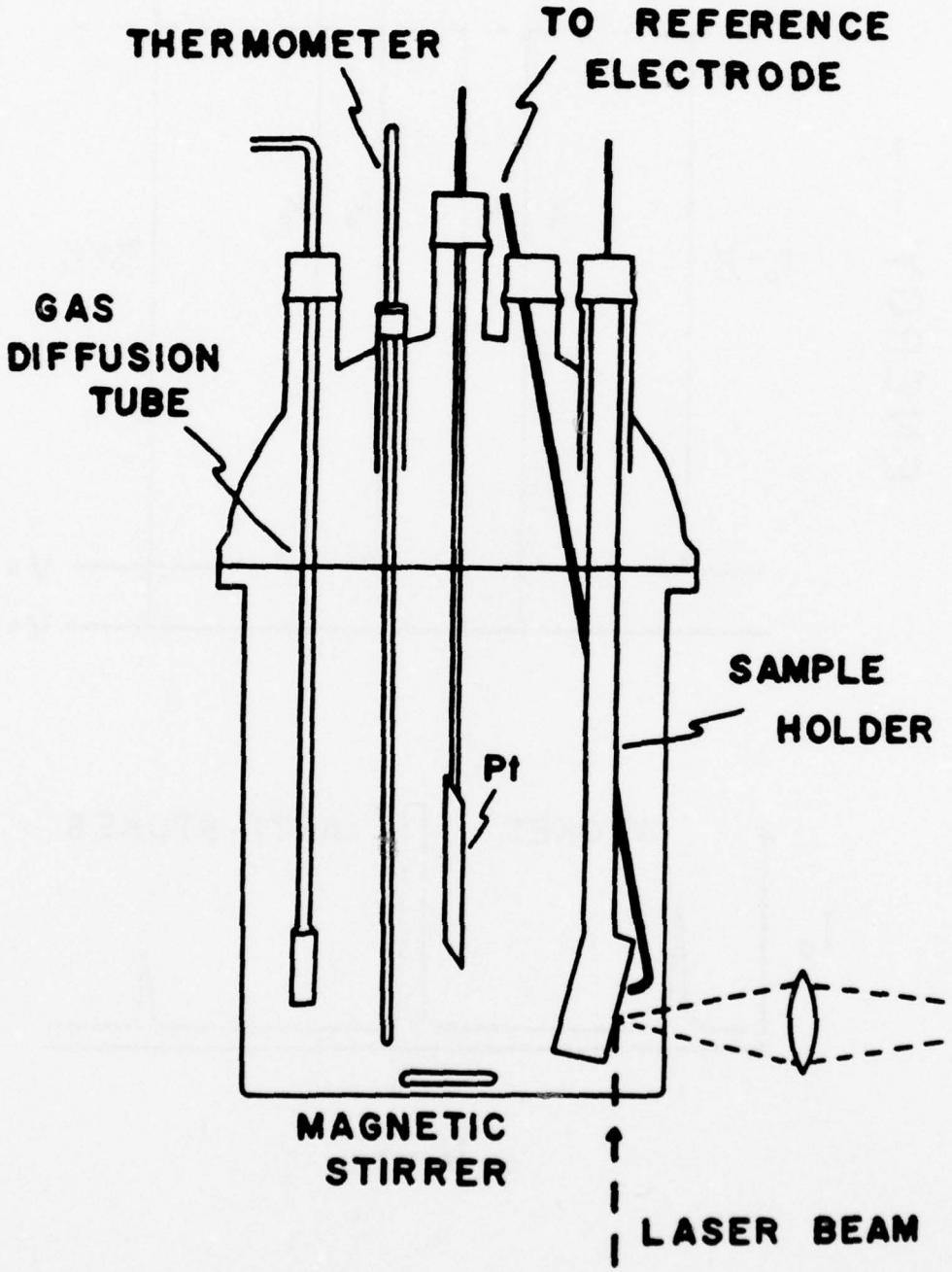
THERMOMETER
TO REFERENCE ELECTRODE
GAS DIFFUSION TUBE
SAMPLE HOLDER
Pt
MAGNETIC STIRRER
LASER BEAM

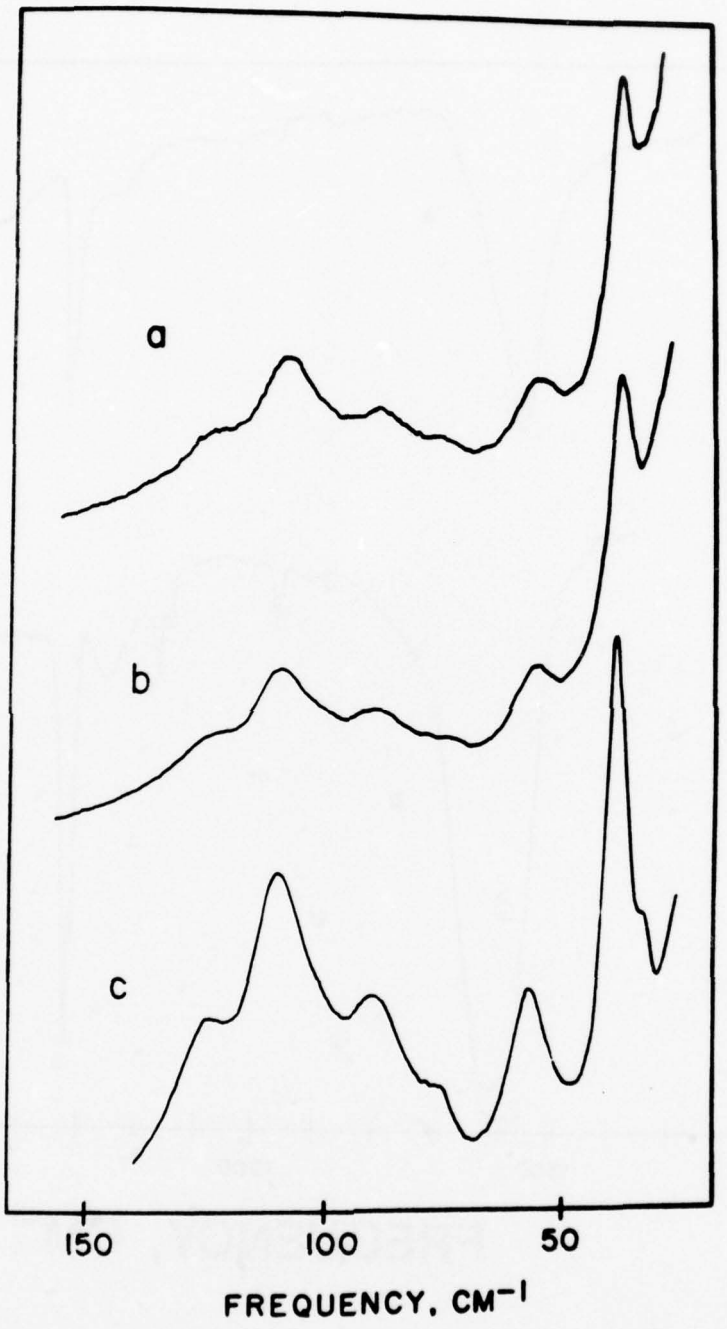
a
b
c
150
100
50
FREQUENCY, CM⁻¹

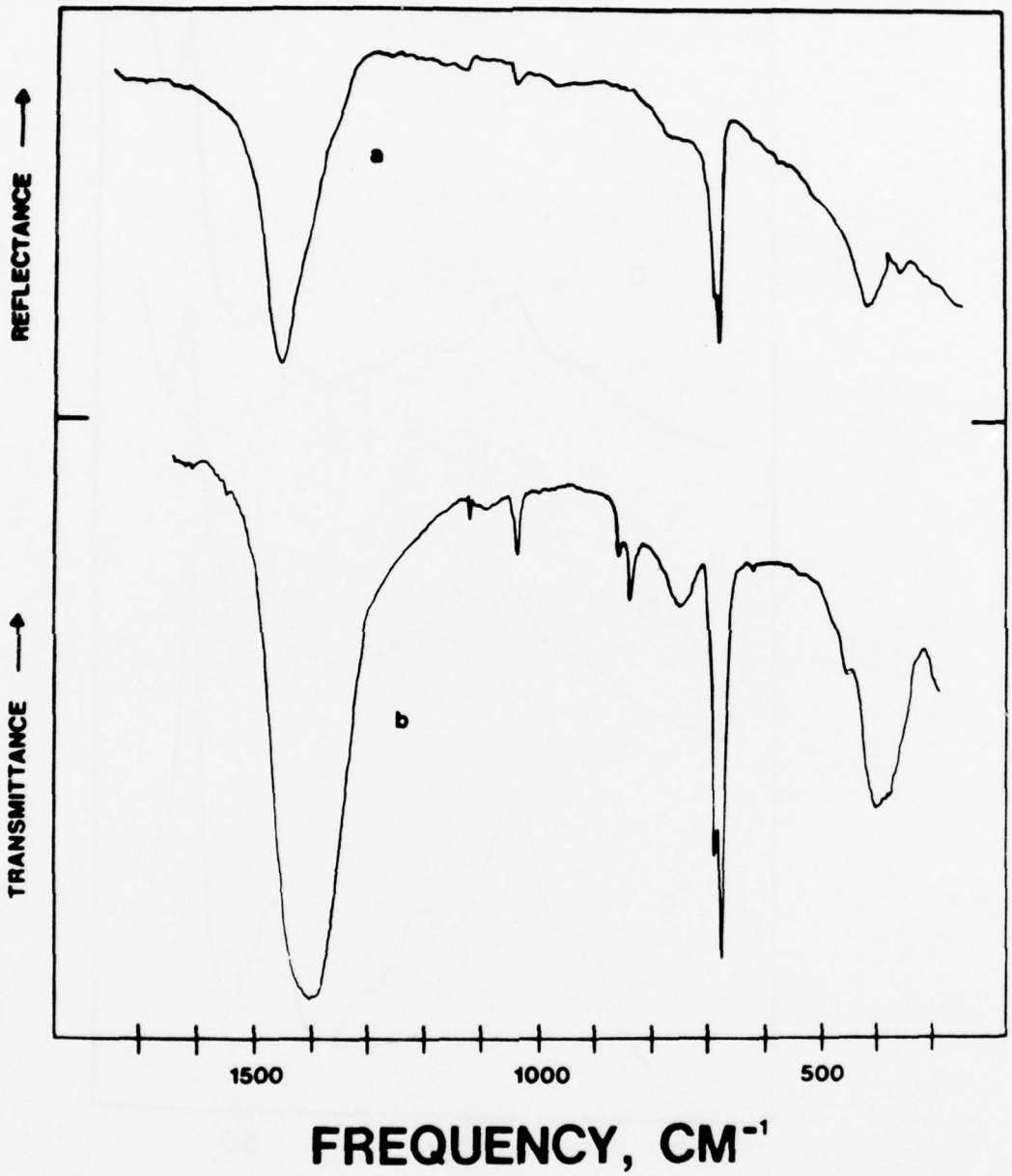
REFLECTANCE
a
TRANSMITTANCE
b
1500
1000
500
FREQUENCY, CM-1

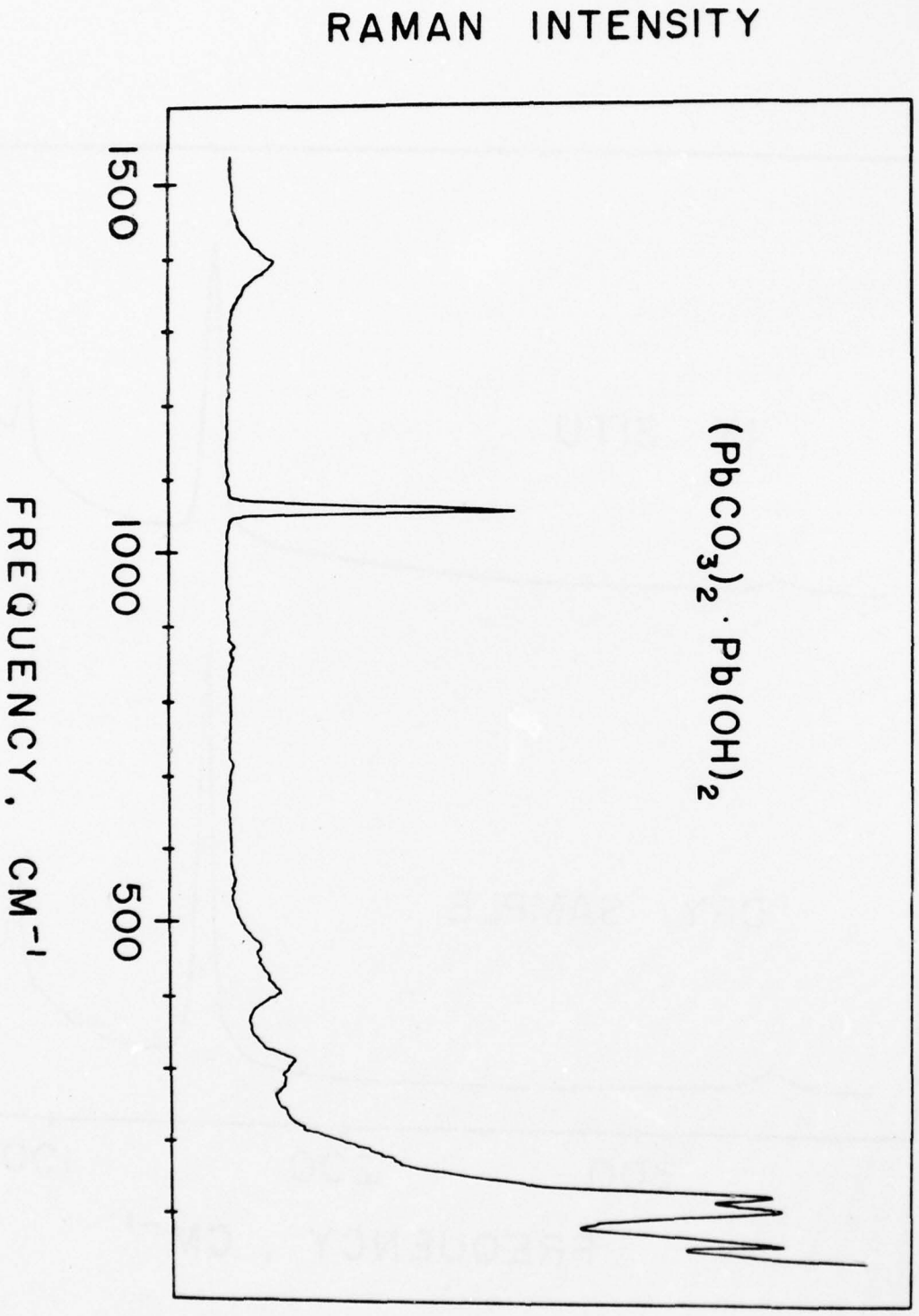
RAMAN INTENSITY
1500
1000
500
FREQUENCY, CM⁻¹
(PbCO3)2 · Pb(OH)2

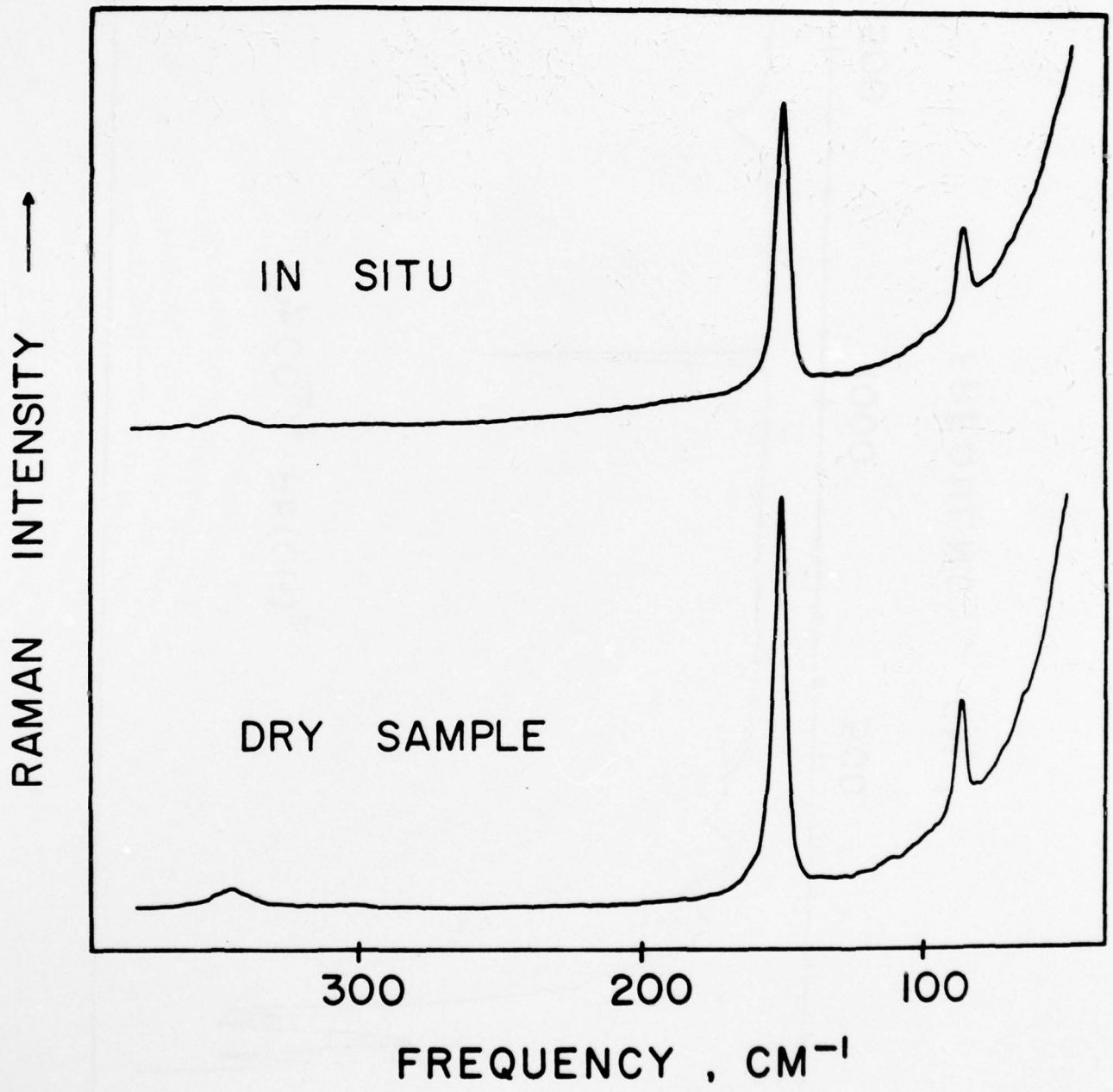
RAMAN INTENSITY
IN SITU
DRY SAMPLE
300
200
100
FREQUENCY , CM⁻¹

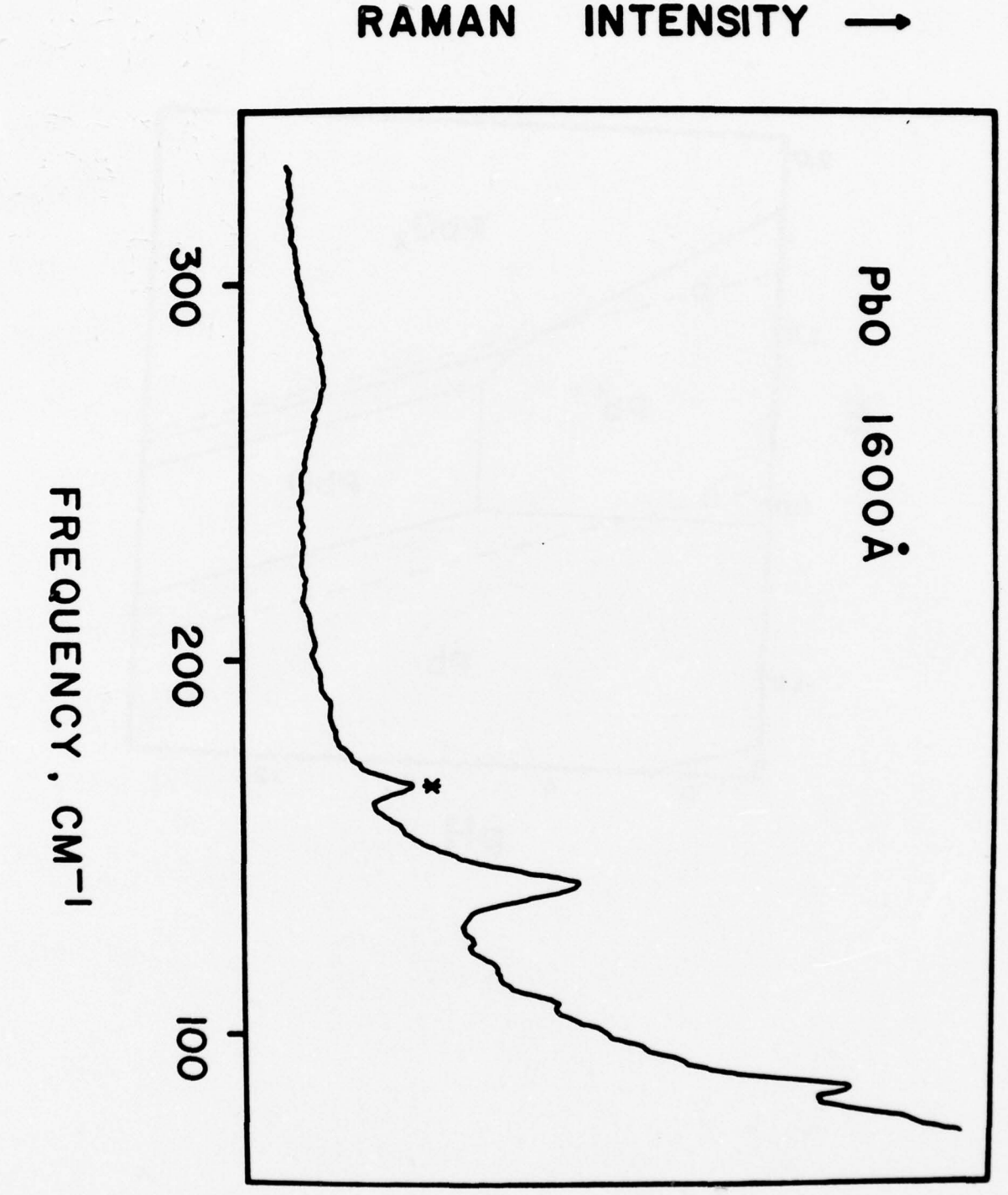
RAMAN INTENSITY →
PbO 1600Å
300
200
100
FREQUENCY, CM⁻¹

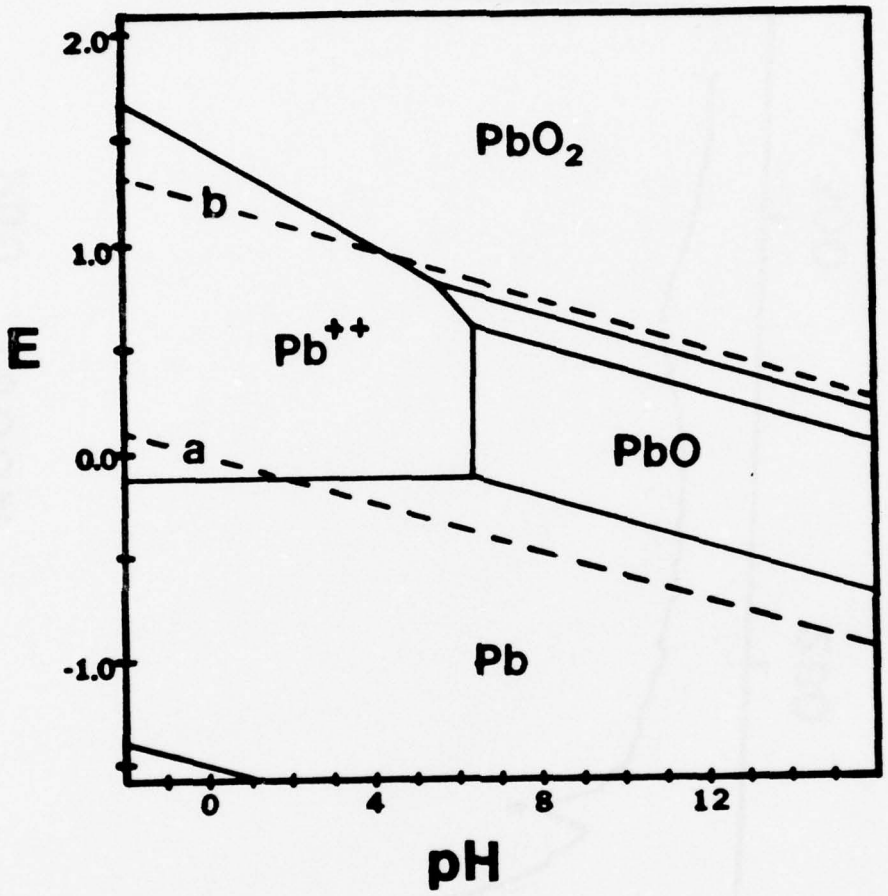
2.0
1.0
0.0
-1.0
E
PbO_2
b
Pb^{++}
a
PbO
Pb
0
4
8
12
pH

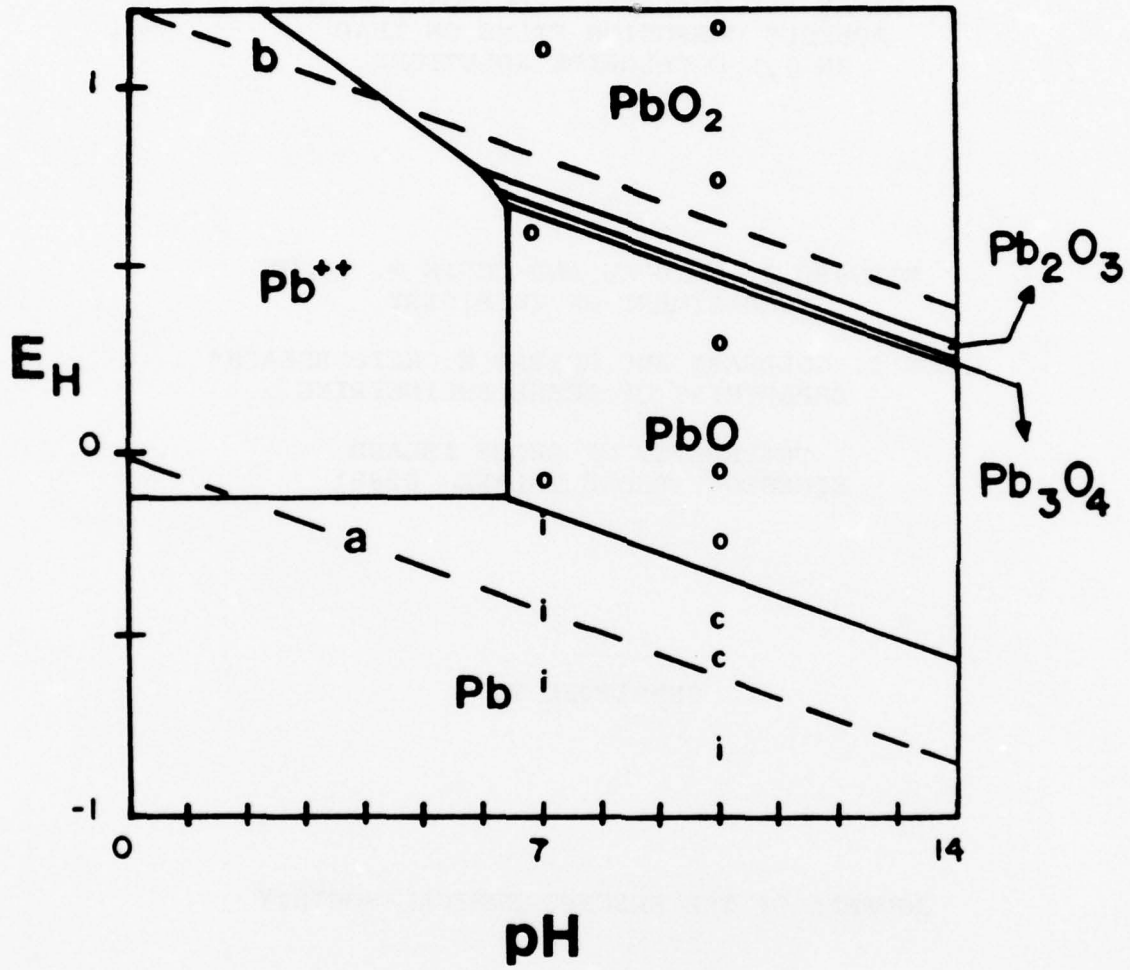
b
a
PbO_2
Pb^{++}
PbO
Pb
Pb_2O_3
Pb_3O_4
E_H
1
0
-1
0
7
14
pH

RAMAN AND INFRARED SPECTROSCOPY OF AQUEOUS CORROSION FILMS ON LEAD IN 0.1 M CHLORIDE SOLUTIONS

RICHARD J. THIBEAU AND CHRIS W. BROWN
DEPARTMENT OF CHEMISTRY

ARNON Z. GOLDFARB AND ROBERT H. HEIDERSBACH*
DEPARTMENT OF OCEAN ENGINEERING

UNIVERSITY OF RHODE ISLAND
KINGSTON, RHODE ISLAND 02881

SUBMITTED TO

JOURNAL OF THE ELECTROCHEMICAL SOCIETY

*ELECTROCHEMICAL SOCIETY ACTIVE MEMBER

ABSTRACT

The Pb-H_2O-Cl Pourbaix diagram was investigated by examining potentiostatically oxidized lead samples using Raman and infrared spectroscopy. The surface films formed in 0.1 M HCl solution were those predicted by the potential-pH diagram. In neutral and basic solutions, the film compositions were not as predicted by thermodynamic calculations, although potentiostatic results agreed very well with potentiodynamic polarization curves. Two polymorphs of PbO were found at different potentials in pH7 solutions, the orthorhombic form at low potentials and the tetragonal form above +0.18 V vs. NHE. Infrared spectra gave indications that orthorhombic PbO is formed by deposition from solution while tetragonal PbO forms from the reaction of water with the metallic lead surface.

INTRODUCTION

Laser Raman spectroscopy is an effective technique for analysis of aqueous corrosion product films on metal surfaces. It can identify insoluble aqueous corrosion products in situ, without removing a sample from its corrosive environment (1).

Raman spectra of relatively thin surface films (50 Å) on metals can be observed (2). Since water is a very weak Raman scatterer, there is little difference between spectra of dry samples and of those immersed in a reactive aqueous solution (1,3). Metal samples can be examined undisturbed in an electrochemical cell while oxidation proceeds under controlled conditions in different regions of a Pourbaix diagram. In situ Raman spectroscopy, in combination with the complementary and more sensitive technique, infrared reflection-absorption spectroscopy, can unambiguously identify insoluble films formed at specific conditions of potential and pH.

A previous report discussed investigations of the Pourbaix diagram for the Pb-H_2O system (1). The present report describes spectroscopic results from exposures of lead under similar conditions with 0.1 M chloride ions added to the solutions in order to identify the effect of the chloride ion on lead oxide surface films.

EXPERIMENTAL

Raman spectra were recorded with a Spex Industries Model 1401 double monochromator using a photon counting detection system. A Coherent Radiation Laboratories Model CR-3 argon ion laser was used as the excitation source. Both the 488.0 and 514.5 nm

wavelength laser lines were used and the power at the sample was approximately 500 mW.

Infrared reflection-absorption spectra were obtained with a Wilks Scientific Corporation Model 9 multiple specular reflection attachment in both the sample and reference beams of a Perkin-Elmer Model 521 infrared spectrophotometer equipped with a grating polarizer. The reflection apparatus was adjusted to give 2 to 4 reflections and a 65° angle of incidence of the infrared beam. Details of the exposure apparatus and instrumentation used in this research are contained in a previous report (1).

Lead foil (1.6 mm thick) supplied by Alfa Products, Inc., at greater than 99.9% purity was used for the investigation. It was cut into 2.8 x 5.7 cm rectangles to fit the sample holder of the electrochemical cell. This size was also required for the infrared reflection attachment. Prior to placing a lead sample in solution, it was immersed in warm, concentrated ammonium acetate solution for 5 minutes to dissolve the outer layer, leaving a clean, silvery surface. The clean sample was washed with distilled water and immediately placed in the exposure solution.

The solutions were sparged with dry nitrogen for 30 minutes before and throughout the electrochemical exposures. The potential of the working electrode, lead, was held constant relative to the saturated calomel reference electrode by a Wenking Model LT73 potentiostat for periods ranging from one to twenty-four hours. Upon completion of an exposure period, an in situ Raman spectrum was recorded. The sample was then removed from the cell, washed thoroughly with distilled water, and allowed to dry in air. The dry sample was returned to the Raman spectrometer for

examination and then analyzed by the infrared spectrophotometer.

The solutions used were made from reagent grade compounds. The acid solution was 0.1 M HCl. The pH7 buffer was a KH_2PO_4-NaOH solution and that for pH10 was a $NaHCO_3$-NaOH mixture, both with KCl added to make the solution 0.1 M in Cl^-. Buffer solutions were desired to maintain pH constant throughout periods of exposure as long as 24 hours but no suitable buffer was available in the strongly acidic region.

RESULTS AND DISCUSSION

The Pourbaix diagram for the Pb-H_2O-Cl system was calculated in the manner used by Appelt (4) but employing more recent thermodynamic data for some species (5). The newer free energy values used in the calculations are given in Table 1. The positions of equilibria between species on the diagram depend strongly on the chloride concentration. A concentration of 0.1 M was chosen for the exposures as a reasonable ionic concentration which should affect oxide film formation. The 0.1 M Cl^- concentration was used in construction of the potential-pH diagram shown in Figure 1.

In order to provide an experimental basis for choosing exposure potentials, as well as the theoretical, thermodynamic basis - the Pourbaix diagram, potentiodynamic polarization curves were recorded for lead in the three solutions selected for exposures. The polarization curves were run with a slowly changing potential, 40 mV/min, to allow the formation of a relatively thick oxide film, as would be encountered in potentiostatic oxidation.

It can be seen from the polarization curves, Figure 2, that there is a definite relation between these curves and the Pourbaix

diagram. The lower oxidative wave occurs at the approximate potential of the predicted $Pb/PbCl_2$ or $Pb/3PbO \cdot PbCl_2$ transitions and the wave at +0.96 V (vs. NHE) in pH10 corresponds roughly to the $3PbO \cdot PbCl_2/PbO_2$ transition. The Pourbaix diagram offers no reason for the waves found at +0.17 V in pH7 or at -0.07 V in pH10, however.

Potentials to be used for lead exposures were chosen so that at least one was located in each region of the theoretical Pourbaix diagram and in all potential regions where the polarization curves indicated the possible formation of different species. The exposure conditions selected and the resulting spectra obtained from these potentiostatic oxidations are summarized in Table 2. The current densities listed are those recorded after current became steady.

pH 1 Exposures: In 0.1 M HCl solution, lead is stable at low potentials while it is oxidized to $PbCl_2$ at higher potentials (3,6). The Raman spectra of lead oxidized at potentials of +0.14 V and higher indicated the presence of a $PbCl_2$ surface layer as shown in Figure 3. The spectrum of the surface film is identical to that of a powder sample of pure $PbCl_2$ with bands at 62, 88, 126, 156 and 178 cm^{-1} (7,8). No infrared spectra of these samples were obtained because lead chloride has no absorption bands in the infrared region examined by the spectrophotometer, 1500-250 cm^{-1} (9). Current densities for these samples were extremely high and the lead quickly became covered with a light gray crystalline coating.

In the region where immunity is predicted, net current flow was in the reducing direction and samples remained clean in appear-

ance. In situ Raman spectra gave no indication of film formation but upon drying both Raman and infrared spectra indicated the presence of orthorhombic PbO on the lead surface. It is unlikely that the PbO was formed by oxidation of the lead under generally reducing conditions, but it is probably the result of dissolved lead being redeposited from the solution as the oxide. It has been suggested (10) that orthorhombic PbO is formed from the plumbous ion by the reaction:

1) $Pb^{++} + H_2O \rightarrow PbO + 2H^+$

Due to the solubility of lead in 1.0 M hydrochloric acid, sufficient quantities of Pb^{++} are present to form orthorhombic PbO films on lead undergoing exposure for several hours.

In the potential region where $PbCl_2$ was formed, a gray coating was deposited on the platinum cathode. After drying, the material gave the Raman spectrum of orthorhombic PbO. Apparently the oxide on the auxiliary electrode was formed by the same dissolution-deposition mechanism as that found on the working electrode.

Raman spectra of the dried cathode coating were recorded in two ways: as a powder in a glass capillary tube, or pressed into a KBr pellet. As shown in Figure 4, the spectra are slightly different for the different sample preparation techniques. While both are spectra of orthorhombic PbO, the pellet spectrum shows impurity bands at 84, 149 and 344 cm^{-1}, the three strong bands of tetragonal PbO, litharge. The same results were obtained with spectra of reagent grade orthorhombic PbO. The grinding required to make a pellet transforms some of the orthorhombic PbO to the lower energy, tetragonal form. The crystal structures of the two

oxides are very similar (11) and at room temperature the tetragonal structure is thermodynamically stable. Orthorhombic PbO is known to be stabilized by the presence of small quantities of various impurity anions (12), which allow it to remain indefinitely without reverting to the tetragonal structure. It is likely that the presence of chloride or some other ion in the solution stabilizes orthorhombic PbO so that it can remain in that form until intensive grinding brings about the transformation.

pH7 Exposures: According to the Pourbaix diagram in Figure 1, controlled potential oxidations of lead in a pH7, 0.1 M chloride solution should show immunity at potentials below -0.26 V vs. NHE, formation of $3PbO \cdot PbCl_2$ between -0.26 V and +0.75 V, and formation of PbO_2 at higher potentials. The predicted compounds were not found experimentally.

In the region where immunity is predicted, i.e., below -0.26 V, the Pourbaix diagram, polarization curve, and spectroscopic results all agree. Potentiostatic exposure resulted in a reducing current, the sample remained shiny and silver in color, and no infrared or Raman bands could be observed.

Above the potential where Pb is the stable species, i.e., -0.34 V according to the polarization curve of Figure 2, an insoluble oxidation product film was formed. Current flow, although small, was in the oxidizing direction. The sample surface darkened and, after a few hours, became dull gray in color. In situ Raman spectra and infrared reflection spectra of sample surfaces indicated that, at potentials between -0.11 V and +0.18 V, orthorhombic PbO was formed. At potentials above +0.18 V, the film consists entirely of tetragonal PbO, whereas exposures at

+0.18 V showed both types present, as spectra show in Figure 5. There was no difficulty in identifying which PbO polymorph was present. While the structures are similar, infrared and Raman spectra of the two polymorphs are markedly different (13,14).

We have no explanation why the two types of PbO should be found at different potentials. The tetragonal form is thermodynamically favored under all conditions at room temperature. It is likely that the weak wave at approximately +0.16 V on the polarization curve indicates a PbO (0) to PbO (+) transition, but such a transition is not reflected in the Pourbaix diagram which is based solely on thermodynamic equilibria.

Infrared spectra indicate that the orthorhombic PbO films may be formed by deposition from the solution. Reflection spectra of orthorhombic PbO films recorded using two different polarizations of the infrared beam were very similar, differing only in intensity (15). However, spectra of tetragonal PbO films had differing relative peak heights depending on polarization. This is shown in Figure 6. This indicates that, while orientation of orthorhombic PbO crystals is probably random, there is probably some long range order to the tetragonal films. Long range order may be expected if the oxide is formed directly on the lead surface by the reaction:

$$2)\quad Pb + H_2O \rightarrow PbO + 2H^+ + 2e^-$$

Thus the tetragonal PbO layer may be aligned with the grain structure of the underlying metal while orthorhombic PbO, formed by a dissolution-deposition route, is random in orientation.

The effect of chloride ions was investigated by conducting exposures at -0.01 V in pH7 solutions of different KCl concentra-

tions: 0.01 M and 0.1 M. In 0.01 M Cl^- solution, the oxidation product detected was tetragonal PbO, the same compound observed in nil chloride exposures (1). In 0.1 M Cl^- orthorhombic PbO was formed. These results indicate that it is indeed the chloride present in solution which allows the formation of the thermodynamically unstable orthorhombic PbO layer.

pH10 Exposures: According to the Pourbaix diagram the results of potentiostatic exposures should be the same in pH10 solutions as in pH7 but, experimentally, they are not. The differences are due, in part, to the composition of the pH10 buffer used. They are also due to the behavior of soluble lead species in basic solutions.

The pH10 buffer, a bicarbonate solution, gave slightly different results from those predicted in the immunity region. As in nil chloride exposures (1), potentials in the region of Pb stability in the potential -pH diagram, but above -0.42 V, gave oxidizing currents and a thin film of basic lead carbonate. The oxidation wave at -0.35 V apparently corresponds to the Pb to $(PbCO_3)_2 \cdot Pb(OH)_2$ transition.

At potentials higher than the carbonate region, tetragonal PbO was found, between -0.07 V and + 0.96 V. No trace of the orthorhombic form was detected. The dissolved lead species, Pb^{++} and $HPbO_2^-$, are in equilibrium at a pH of 9.34 (16). In more basic solutions only $HPbO_2^-$ is present, the Pb^{++} needed to make orthorhombic PbO according to the mechanism of reaction 1) is not present.

Although the transition to a higher oxidation state predicted by the Pourbaix diagram would give PbO_2, none could be de-

tected. Instead a thick, nonprotective film of Pb_3O_4 was formed at potentials above the +0.96 V wave. The Raman spectrum of this compound has not previously been reported but the composition of the film was confirmed by comparison of its Raman spectrum with that of the pure compound, as shown in Figure 7, and by its infrared spectrum which agrees with a previously reported IR spectrum of Pb_3O_4 (17).

CONCLUSIONS

In situ Raman spectroscopy and infrared reflection-absorption spectroscopy are excellent methods for the experimental investigation of Pourbaix diagrams. Examining two different potential-pH diagrams, we have found considerable difference in the oxidation of lead between nil chloride and 0.1 M chloride solutions. Orthorhombic PbO and Pb_3O_4 were formed only in the presence of chlorides. The relationship between the tetragonal and orthorhombic PbO polymorphs is not well understood. Some potentials and chloride concentrations result in formation of one type while other potentials or concentrations give the other.

The experimental results of potentiostatic oxidations agree very well with slow potentiodynamic polarization curves but only partially with the calculated Pourbaix diagram. The major difference is that, where $3PbO \cdot PbCl_2$ is predicted, PbO was found. The compound $3PbO \cdot PbCl_2$, which probably exists as $3Pb(OH)_2 \cdot PbCl_2$ or $(Pb_8(OH)_{12})_n\ Cl_{4n}$, has a somewhat different spectrum (3) and should have been easily detected. In calculating the regions of the diagram, the presence of dissolved substances other than lead or chloride species was not considered. The presence of the

buffer solutions may account for the discrepancies between experimental results and those predicted by the Pourbaix diagram. In 1.0 M HCl, a simpler solution where no unaccounted for compounds were present, the Pourbaix diagram, polarization curve, and potentiostatic exposures all agreed.

ACKNOWLEDGEMENT

The authors thank the Department of the Navy, Office of Naval Research, for support of this research under contract N0014-76-C-0889.

FIGURE CAPTIONS

Figure 1. Potential-pH diagram of the system Pb-H_2O-Cl at 25° C for $a_{Cl} = 0.1$.

Figure 2. Potentiodynamic polarization curves for lead, scan rate 40 mV/min.

Figure 3. Raman spectrum of the surface film on lead exposed to 0.1 M HCl at +0.69 V vs. SHE for 2.5 hours.

Figure 4. Raman spectra of dried material from the Pt cathode after lead exposure at +1.09 V in 0.1 M HCl for 17 hours. Bands marked "t" are due to tetragonal PbO.

Figure 5. In situ Raman spectra of lead surfaces exposed to pH7, 0.1 M chloride solutions for 18 hours at +0.68 V, +0.68 V, +0.18 V and -0.11 V vs. SHE. The spectra indicate tetragonal, tetragonal plus orthorhombic, and orthorhombic PbO films respectively. The feature marked with an asterisk is a grating ghost.

Figure 6. Infrared reflection spectra of a tetragonal PbO surface film with two different polarizations of the incident beam. The PbO was formed by exposure of lead in pH10, 0.1 M chloride solution at +0.49 V for 17 hours.

Figure 7. Raman spectra of a KBr pellet of Pb_3O_4 and of the surface of lead after exposure in pH10, 0.1 M chloride solution at +1.07 V for 18 hours.

REFERENCES

1. R.J. Thibeau, C.W. Brown, A.Z. Goldfarb, and P.H. Heidersbach, submitted to J. Electrochem. Soc.

2. R.G. Greenler and T.L. Slager, Spectrochim. Acta, 29A, 193 (1973).

3. E.S. Reid, R.P. Cooney, P.J. Hendra, and M. Fleischmann, J. Electroanal. Chem., 80, 405 (1977).

4. K. Appelt, Electrochim. Acta, 13, 1521 (1968).

5. D.D. Wagman, W.H. Evans, V.B. Parker, I. Halow, S.M. Bailey, and R.H. Schumm, NBS Technical Note 270-3, U.S. Government Printing Office, 1975.

6. R.G. Barradas, K. Belinko, and J. Ambrose, Can. J. Chem., 53, 389 (1975).

7. L.A. Isupova and E.V. Sobolev, Zh. Struct. Khim., 9, 324 (1968).

8. G.A. Ozin, Can. J. Chem., 48, 2931 (1976).

9. T.S. Moss and A.G. Peacock, Infrared Phys., 1, 104 (1961).

10. J. Burbank, J. Electrochem. Soc., 106, 369 (1959).

11. E.W. Abel, Comprehensive Inorganic Chemistry, J.C. Bailar, H.J. Emeleus, R. Nyholm, and A.F. Trotman-Dickenson, eds., Pergamon, 1973, vol. 2, p. 119.

12. W. Kwestroo, J. DeJonge, and P.H.G.M. Vromans, J. Inorg. Nucl. Chem., 29, 39(1967).

13. J.D. Donaldson, M.T. Donoghue, and S.D. Ross, Spectrochim. Acta. 30A, 1967 (1974).

14. D.M. Adams and D.C. Stevens, J.C.S. Dalton, 1977, 1096 (1977).

15. R.G. Greenler, J. Chem. Phys., 44, 310 (1966).

16. M. Pourbaix, Atlas of Electrochemical Equilibria, Pergamon, New York, 1966, pp. 485-492.

17. N.T. McDevitt and W.L. Baun, Spectrochim. Acta, 20, 799 (1964).

TABLE 1. REVISED FREE ENERGY VALUES USED TO CALCULATE POURBAIX DIAGRAM

SUBSTANCE	ΔG_f^o (cal/mole)	
	NBS (5)	Used by Appelt (5)
OH^-	-37,594	-37,595
Cl^-	-31,372	-31,350
$PbCl_2$	-75,080	-75,040
$3PbO \cdot PbCl_2$	-224,686	-225,000

TABLE 2. POTENTIOSTATIC EXPOSURES CONDUCTED IN 0.1 M CHLORIDE SOLUTIONS

Solution pH	Potential V vs. SHE	Current $\mu a/cm^2$	Surface Film Spectrum
1	-0.46	11.2[a]	none[b]
1	-0.30	120[a]	none[b]
1	+0.14	7300	$PbCl_2$
1	+0.69	6800	$PbCl_2$
1	+1.09	10000	$PbCl_2$
7	-0.62	[a]	none
7	-0.11	20	PbO (o)
7	-0.01	22	PbO (o)
7	+0.18	19	PbO (o++)
7	+0.49		PbO (+)
7	+0.68	12	PbO (+)
7	+0.99	22	PbO (+)
10	-0.42	[a]	none
10	-0.26	6.5	$(PbCO_3)_2 \cdot Pb(OH)_2$
10	-0.01	14	PbO (+)
10	+0.08	12	PbO (+)
10	+0.49		PbO (+)
10	+0.74	34	PbO (+)
10	+1.07	28	Pb_3O_4

a. current flow in reducing direction

b. some orthorhombic PbO found on dried sample

(o) indicates orthorhombic structure

(+) indicates tetragonal structure

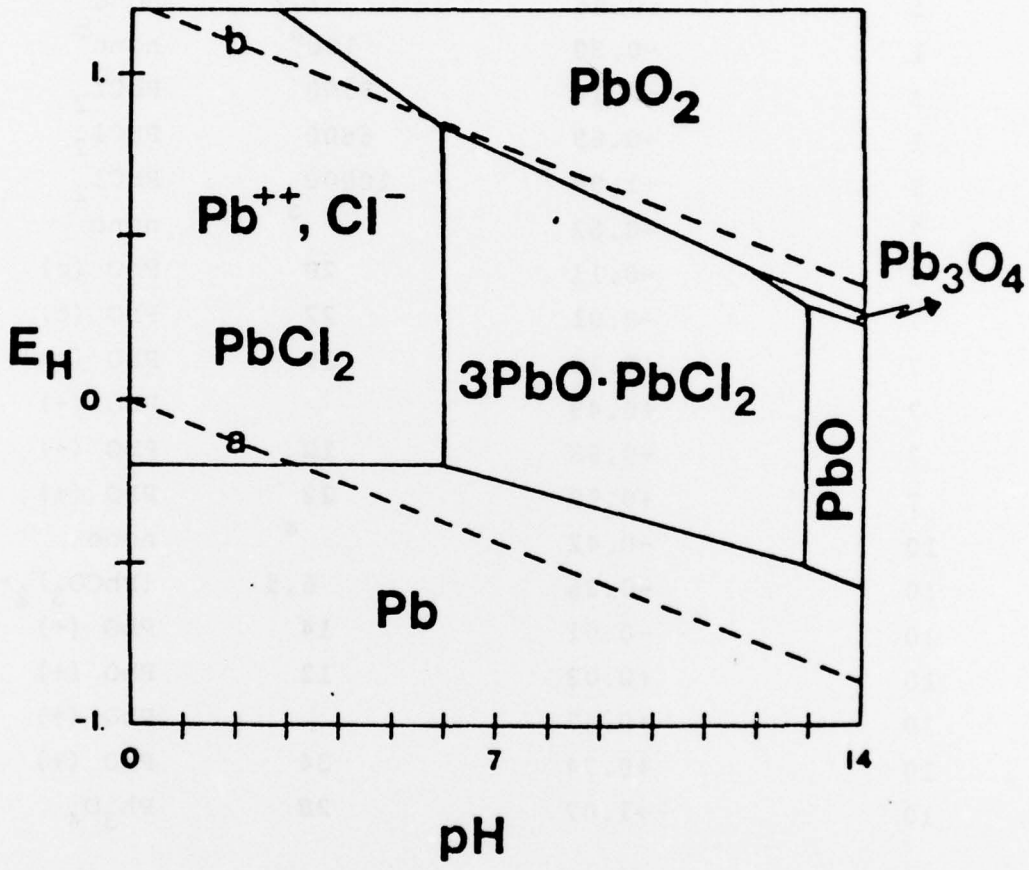
b
a
1.
0
-1.
E_H
PbO_2
Pb^{++}, Cl^-
$PbCl_2$
$3PbO \cdot PbCl_2$
Pb_3O_4
PbO
Pb
0
7
14
pH

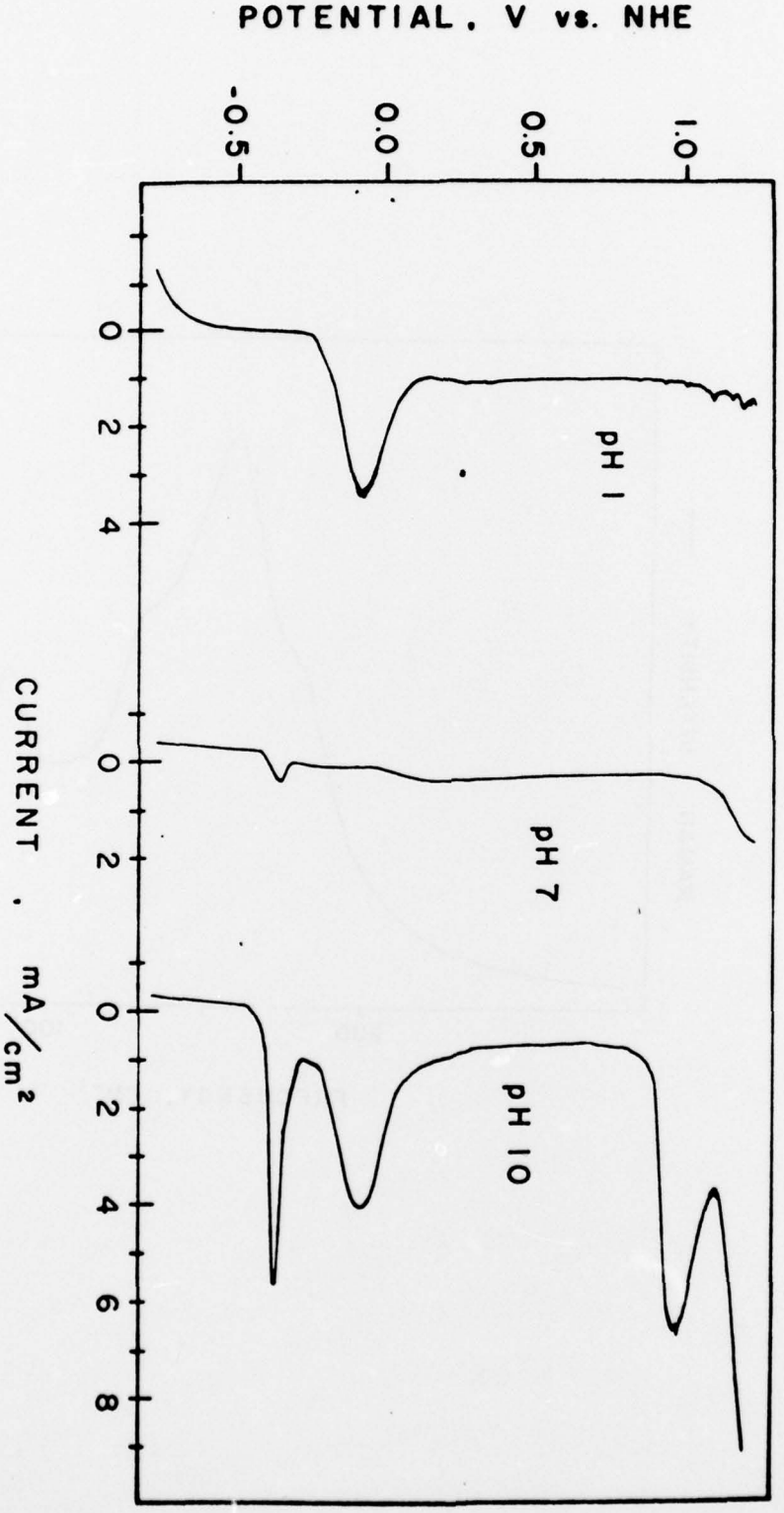
POTENTIAL, V vs. NHE
-0.5
0.0
0.5
1.0
0
2
4
pH 1
0
2
pH 7
0
2
4
6
8
pH 10
CURRENT, mA/cm²

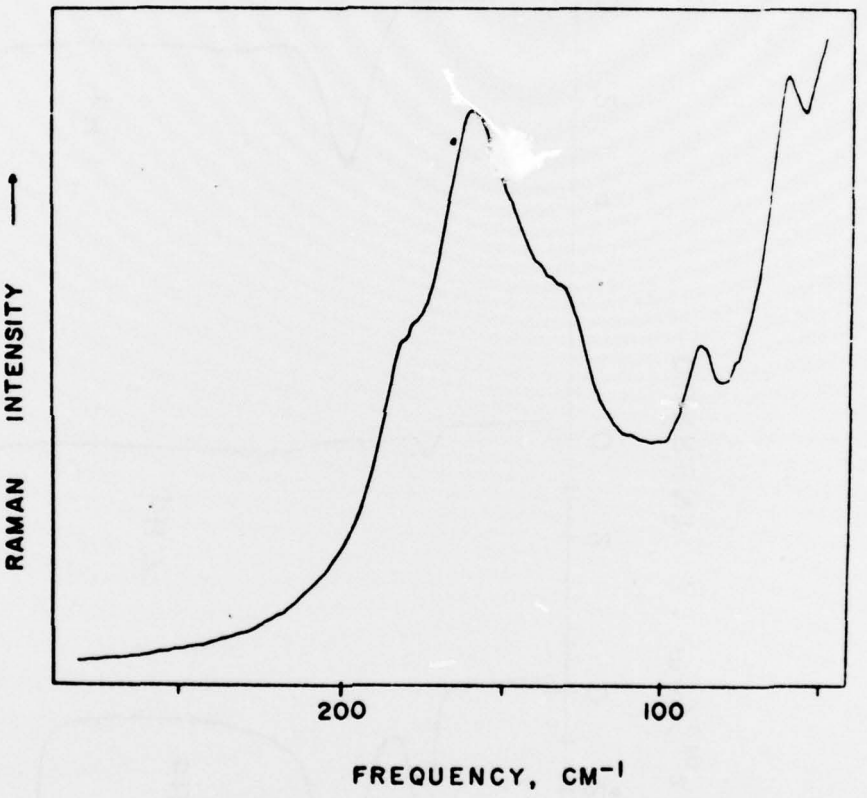
RAMAN INTENSITY
200
100
FREQUENCY, CM⁻¹

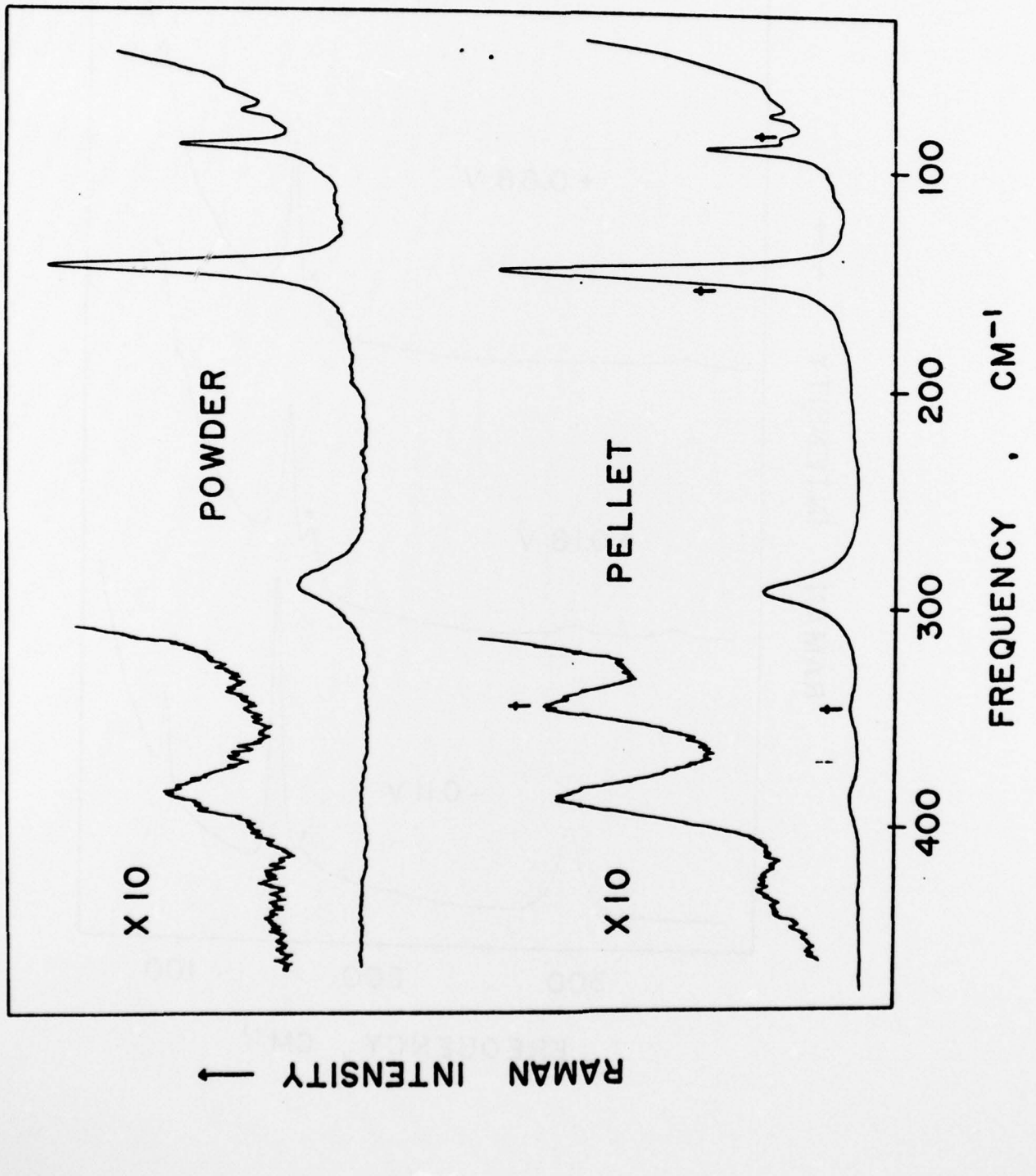
POWDER
PELLET
X 10
X 10
100
200
300
400
FREQUENCY , CM⁻¹
RAMAN INTENSITY

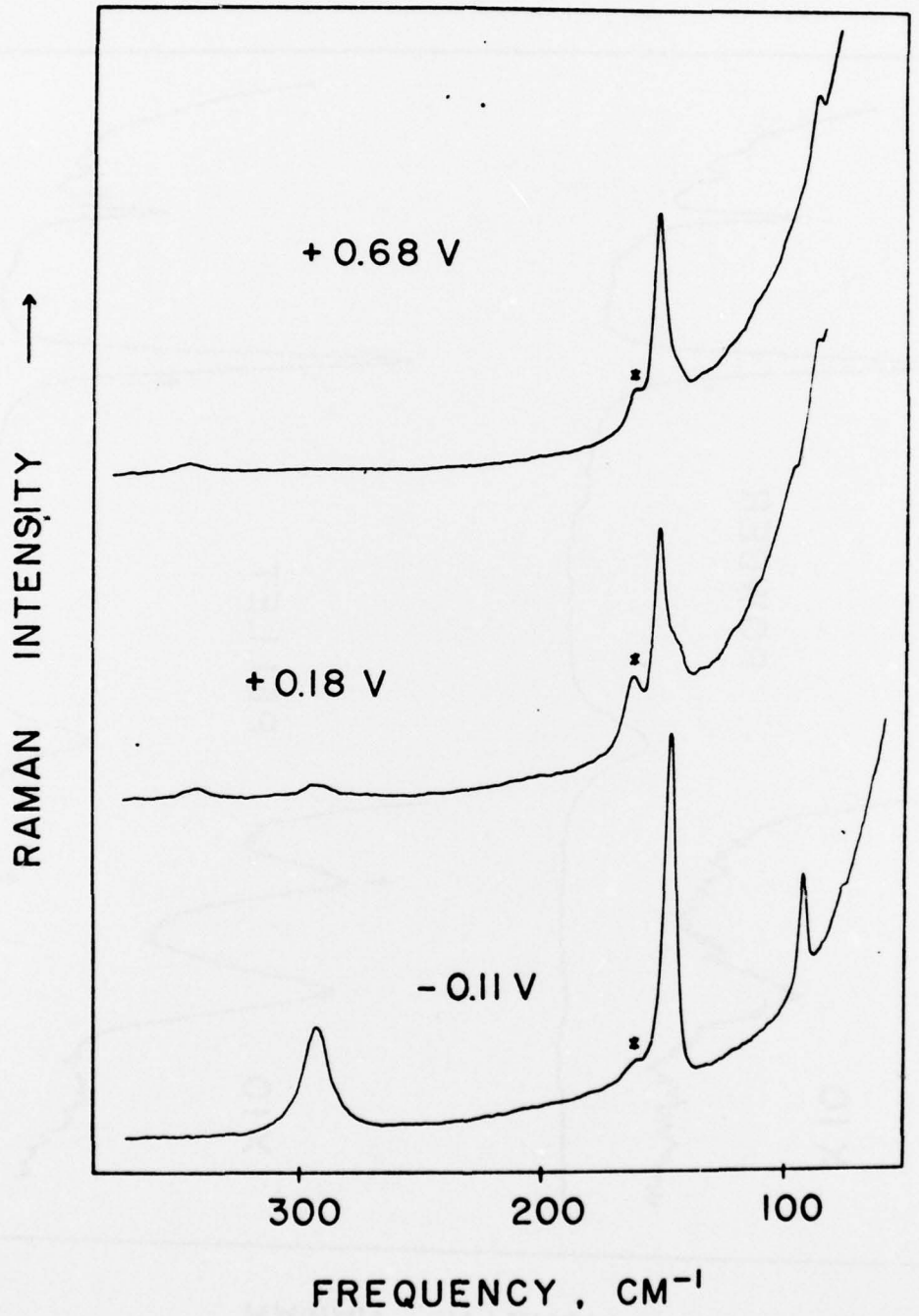
+0.68 V
+0.18 V
-0.11 V
RAMAN INTENSITY
300
200
100
FREQUENCY, CM⁻¹

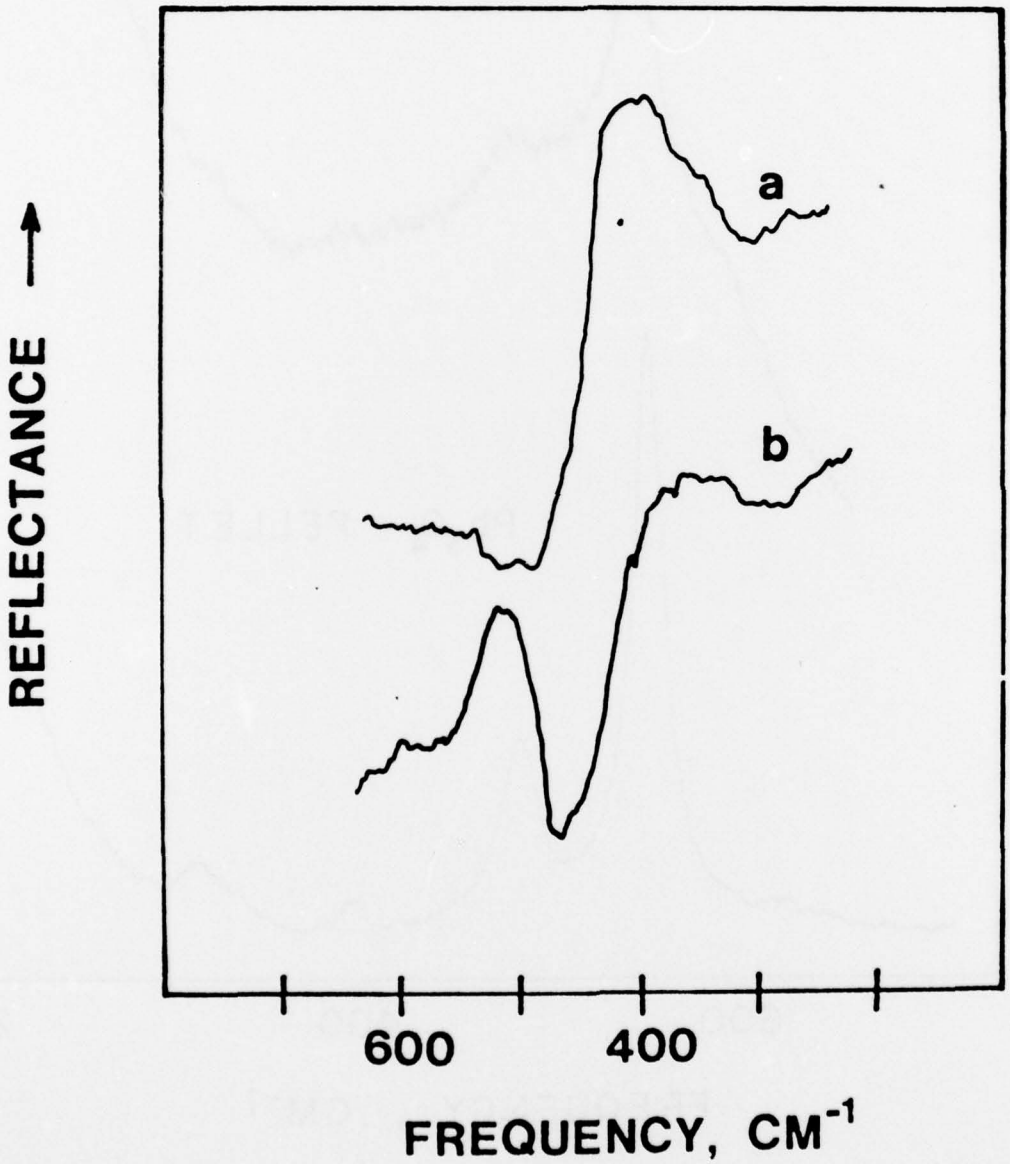
REFLECTANCE →
a
b
600
400
FREQUENCY, CM^{-1}

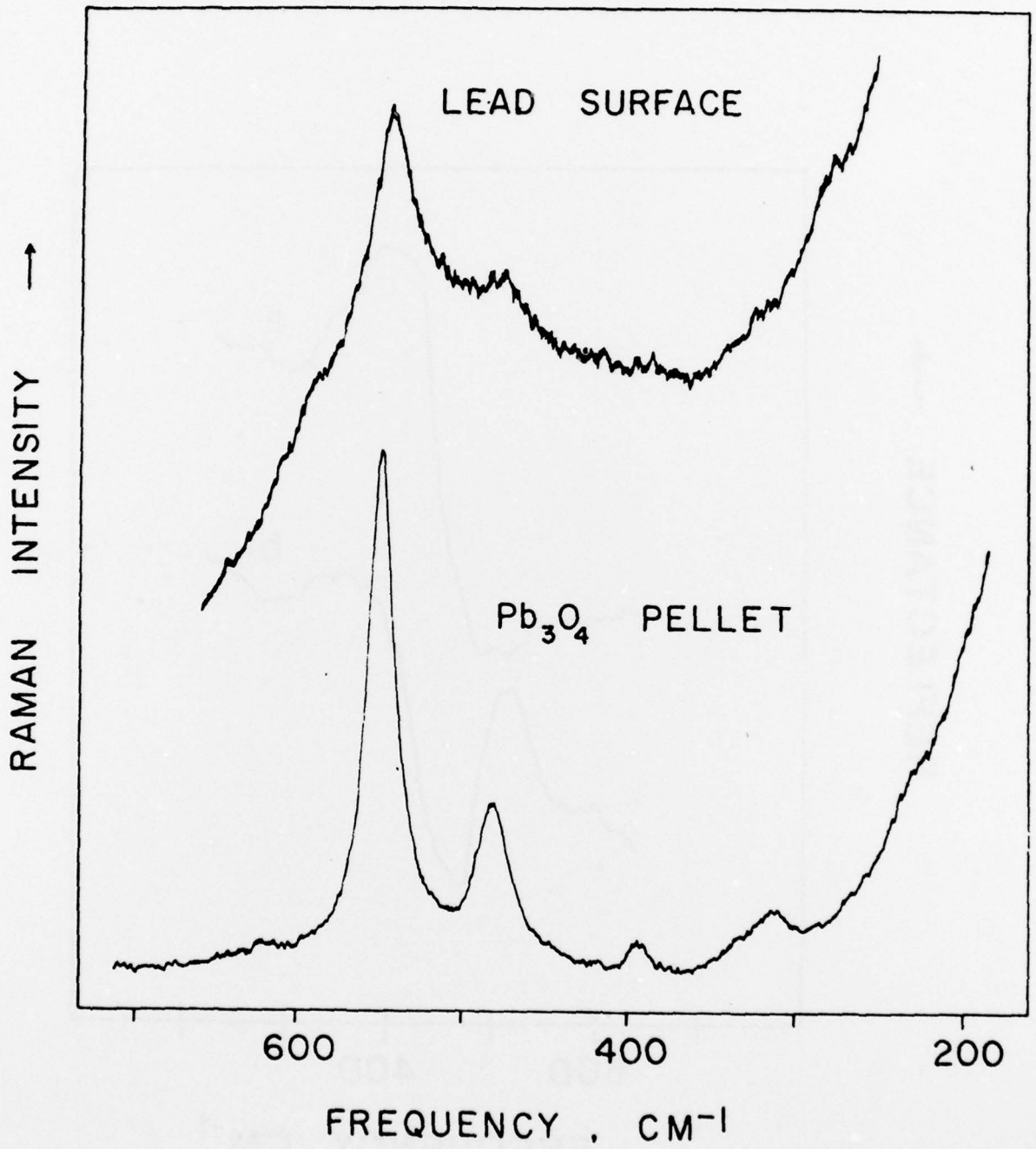
LEAD SURFACE
Pb_3O_4 PELLET
RAMAN INTENSITY →
600
400
200
FREQUENCY , CM^{-1}

BASIC DISTRIBUTION LIST

Technical and Summary Reports April 1978

Organization	Copies
Defense Documentation Center Cameron Station Alexandria, VA 22314	12
Office of Naval Research Department of the Navy 800 N. Quincy Street Arlington, VA 22217	
ATTN: Code 471	1
Code 102	1
Code 470	1
Commanding Officer Office of Naval Research Branch Office Building 114, Section D 666 Summer Street Boston, MA 02210	1
Commanding Officer Office of Naval Research Branch Office 536 South Clark Street Chicago, IL 60605	1
Office of Naval Research San Francisco Area Office 760 Market Street, Room 447 San Francisco, CA 94102	1
Naval Research Laboratory Washington, DC 20375	
ATTN: Codes 6000	1
6100	1
6300	1
6400	1
2627	1
Naval Air Development Center Code 302 Warminster, PA 18964 ATTN: Mr. F. S. Williams	1
Naval Air Propulsion Test Center Trenton, NJ 08628 ATTN: Library	1
Naval Construction Batallion Civil Engineering Laboratory Port Hueneme, CA 93043 ATTN: Materials Division	1
Naval Electronics Laboratory San Diego, CA 92152 ATTN: Electron Materials Sciences Division	1
Naval Missile Center Materials Consultant Code 3312-1 Point Mugu, CA 92041	1
Commanding Officer Naval Surface Weapons Center White Oak Laboratory Silver Spring, MD 20910 ATTN: Library	1
David W. Taylor Naval Ship Research and Development Center Materials Department Annapolis, MD 21402	1
Naval Undersea Center San Diego, CA 92132 ATTN: Library	1
Naval Underwater System Center Newport, RI 02840 ATTN: Library	1
Naval Weapons Center China Lake, CA 93555 ATTN: Library	1
Naval Postgraduate School Monterey, CA 93940 ATTN: Mechanical Engineering Department	1

BASIC DISTRIBUTION LIST (cont'd)

Organization	Copies
Naval Air Systems Command Washington, DC 20360 ATTN: Codes 52031 52032	1
Naval Sea System Command Washington, DC 20362 ATTN: Code 035	1
Naval Facilities Engineering Command Alexandria, VA 22331 ATTN: Code 03	1
Scientific Advisor Commandant of the Marine Corps Washington, DC 20380 ATTN: Code AX	1
Naval Ship Engineering Center Department of the Navy Washington, DC 20360 ATTN: Code 6101	1
Army Research Office P.O. Box 12211 Triangle Park, NC 27709 ATTN: Metallurgy & Ceramics Program	1
Army Materials and Mechanics Research Center Watertown, MA 02172 ATTN: Research Programs Office	1
Air Force Office of Scientific Research Bldg. 410 Bolling Air Force Base Washington, DC 20332 ATTN: Chemical Science Directorate	1
Electronics & Solid State Sciences Directorate	1
Air Force Materials Laboratory Wright-Patterson AFB Dayton, OH 45433	1
Library Building 50, Rm 134 Lawrence Radiation Laboratory Berkeley, CA	1

Organization	Copies
NASA Headquarters Washington, DC 20546 ATTN: Code RRM	1
NASA Lewis Research Center 21000 Brookpark Road Cleveland, OH 44135 ATTN: Library	1
National Bureau of Standards Washington, DC 20234 ATTN: Metallurgy Division	1
Inorganic Materials Div.	1
Director Applied Physics Laboratory University of Washington 1013 Northeast Forthieth Street Seattle, WA 98105	1
Defense Metals and Ceramics Information Center Battelle Memorial Institute 505 King Avenue Columbus, OH 43201	1
Metals and Ceramics Division Oak Ridge National Laboratory P.O. Box X Oak Ridge, TN 37380	1
Los Alamos Scientific Laboratory P.O. Box 1663 Los Alamos, NM 87544 ATTN: Report Librarian	1
Argonne National Laboratory Metallurgy Division P.O. Box 229 Lemont, IL 60439	1
Brookhaven National Laboratory Technical Information Division Upton, Long Island New York 11973 ATTN: Research Library	1
Office of Naval Research Branch Office 1030 East Green Street Pasadena, CA 91106	1

C
April 1978

SUPPLEMENTARY DISTRIBUTION LIST

Technical and Summary Reports

Dr. T. R. Beck
Electrochemical Technology Corporation
10035 31st Avenue, NE
Seattle, Washington 98125

Professor I. M. Bernstein
Carnegie-Mellon University
Schenley Park
Pittsburgh, Pennsylvania 15213

Professor H. K. Birnbaum
University of Illinois
Department of Metallurgy
Urbana, Illinois 61801

Dr. Otto Buck
Rockwell International
1049 Camino Dos Rios
P.O. Box 1085
Thousand Oaks, California 91360

Dr. David L. Davidson
Southwest Research Institute
8500 Culebra Road
P.O. Drawer 28510
San Antonio, Texas 78284

Dr. D. J. Duquette
Department of Metallurgical Engineering
Rensselaer Polytechnic Institute
Troy, New York 12181

Professor R. T. Foley
The American University
Department of Chemistry
Washington, D.C. 20016

Mr. G. A. Gehring
Ocean City Research Corporation
Tennessee Avenue & Beach Thorofare
Ocean City, New Jersey 08226

Dr. J. A. S. Green
Martin Marietta Corporation
1450 South Rolling Road
Baltimore, Maryland 21227

Professor R. H. Heidersbach
University of Rhode Island
Department of Ocean Engineering
Kingston, Rhode Island 02881

Professor H. Herman
State University of New York
Material Sciences Division
Stony Brook, New York 11794

Professor J. P. Hirth
Ohio State University
Metallurgical Engineering
Columbus, Ohio 43210

Dr. D. W. Hoeppner
University of Missouri
College of Engineering
Columbia, Missouri 65201

Dr. E. W. Johnson
Westinghouse Electric Corporation
Research and Development Center
1310 Beulah Road
Pittsburgh, Pennsylvania 15235

Professor R. M. Latanision
Massachusetts Institute of Technology
77 Massachusetts Avenue
Room E19-702
Cambridge, Massachusetts 02139

Dr. F. Mansfeld
Rockwell International Science Center
1049 Camino Dos Rios
P.O. Box 1085
Thousand Oaks, California 91360

Professor A. E. Miller
University of Notre Dame
College of Engineering
Notre Dame, Indiana 46556

C
April 1978

SUPPLEMENTARY DISTRIBUTION LIST
(Continued)

Professor H. W. Pickering
Pennsylvania State University
Department of Material Sciences
University Park, Pennsylvania 16802

Professor R. W. Staehle
Ohio State University
Department of Metallurgical Engineering
Columbus, Ohio 43210

Dr. E. A. Starke, Jr.
Georgia Institute of Technology
School of Chemical Engineering
Atlanta, Georgia 30332

Dr. Barry C. Syrett
Stanford Research Institute
333 Ravenswood Avenue
Menlo Park, California 94025

Dr. R. P. Wei
Lehigh University
Institute for Fracture and
Solid Mechanics
Bethlehem, Pennsylvania 18015

Professor H. G. F. Wilsdorf
University of Virginia
Department of Materials Science
Charlottesville, Virginia 22903

August 1978

SUPPLEMENTARY DISTRIBUTION LIST

Technical and Summary Reports

People and organizations who have requested copies of reports on this research.

Dr. F.P. Mertlas
Department of Energy and Environment
Building 815
Upton, NY 11973

Dr. B. Vyas
Brookhaven National Laboratory
Building 703
Upton, NY 11973

Dr. Henry White
Physics Department
University of Missouri - Columbia
Columbia, MO 65211

Dr. M.J. Graham
National Research Council of Canada
Division of Chemistry
Ottawa, Ontario
Canada K1A OR9

Dr. B.J. Berkowitz
Corporate Research Laboratories
Exxon Research and Engineering Company
P.O. Box 45
Linden, NJ 07036

Dr. S. Gottesfeld
Bell Laboratories
600 Mountain Avenue
Murray Hill, NJ 07974

Dr. Jeff Perkins
Liason Scientist, Metallurgy
Office of Naval Research
Branch Office, London
Box 39
FPO New York 09510

T.E. Evans
Inco Europe, Ltd.
European R & D Centre
Wiggin Street, Birmingham
B160AJ
England

Dr. N. Sato
Faculty of Engineering
Hokkaido University
Kita-Ku, Sapporo, 060
Japan

Dr. K. Sugimoto
Department of Metallurgy
Tohoku University

Distribution List - ONR

Martin W. Kendig
Corrosion Science Group
Department of Nuclear Energy
Brookhaven National Laboratory
Upton, NY 11973

A.S. (Bert) Krisher
Engineering Fellow
Materials Technology
Monsanto
Corporate Engineering Department
Monsanto Company
800 N. Lindbergh Boulevard
St. Louis, Missouri 63166

Tom E. Furtak
Leader, Electrochemistry Group
Solid State Physics Division
Ames Laboratory
U.S. Department of Energy
Iowa State University
Ames, Iowa 50011

Alan G. Miller, Ph.D.
Analytical Specialist Engineer
Boeing Materials Technology
Boeing Commercial Airplane Co.
P.O. Box 3707
MS 73-43
Seattle, WA 98124